THE JOURNAL OF BIOLOGICAL CHEMISTRY VOL. 289, NO. 10, pp. 6565–6580, March 7, 2014

Structure and Immunogenicity of a Peptide Vaccine, Including the Complete HIV-1 gp41 2F5 Epitope

*IMPLICATIONS FOR ANTIBODY RECOGNITION MECHANISM AND IMMUNOGEN DESIGN**

Received for publication, October 17, 2013, and in revised form, December 30, 2013 Published, JBC Papers in Press, January 15, 2014, DOI 10.1074/jbc.M113.527747

Soraya Serrano[‡1,2], Aitziber Araujo[§1,3], Beatriz Apellániz[§], Steve Bryson[¶‖], Pablo Carravilla[§], Igor de la Arada[§], Nerea Huarte[§], Edurne Rujas[§3], Emil F. Pai[¶‖4], José L. R. Arrondo[§], Carmen Domene[‡‡5], María Angeles Jiménez[‡6], and José L. Nieva[§7]**

*From the [‡]Institute of Physical Chemistry "Rocasolano," Consejo Superior de Investigaciones Científicas (IQFR-CSIC), Serrano 119, E-28006 Madrid, Spain, the [§]Biophysics Unit, Consejo Superior de Investigaciones Científicas and University of the Basque Country (CSIC-UPV/EHU) and Department of Biochemistry and Molecular Biology, University of the Basque Country (UPV/EHU), P. O. Box 644, 48080 Bilbao, Spain, the [¶]Departments of Biochemistry, Medical Biophysics, and Molecular Genetics, University of Toronto, Toronto, Ontario M5S 1A8, Canada, [‖]The Campbell Family Institute for Cancer Research, Ontario Cancer Institute/University Health Network, Toronto, Ontario M5G 1L7, Canada, the **Chemistry Research Laboratory, Mansfield Road, University of Oxford, Oxford OX1 3TA, United Kingdom, and the [‡‡]Department of Chemistry, King's College London, Franklin-Wilkins Building, 150 Stamford Street, London SE1 9NH, United Kingdom*

Background: HIV-1 vaccines should elicit broadly neutralizing antibodies as the gp41 "membrane-proximal external region" targeting MAb2F5.
Results: NMR disclosed unprecedented 2F5 peptide-epitope structures. Although overall conformation was preserved in different adjuvants, recovered antibodies after vaccination were functionally different.
Conclusion: Membrane-inserted helical oligomers may encompass effective 2F5 peptide vaccines.
Significance: Disclosing the structures that generate 2F5-like antibodies may guide future vaccine development.

The membrane-proximal external region (MPER) of gp41 harbors the epitope recognized by the broadly neutralizing anti-HIV 2F5 antibody, a research focus in HIV-1 vaccine development. In this work, we analyze the structure and immunogenic properties of MPERp, a peptide vaccine that includes the following: (i) the complete sequence protected from proteolysis by the 2F5 paratope; (ii) downstream residues postulated to establish weak contacts with the CDR-H3 loop of the antibody, which are believed to be crucial for neutralization; and (iii) an aromatic rich anchor to the membrane interface. MPERp structures solved in dodecylphosphocholine micelles and 25% 1,1,1,3,3,3-hexafluoro-2-propanol (v/v) confirmed folding of the complete 2F5 epitope within continuous kinked helices. Infrared spectroscopy (IR) measurements demonstrated the retention of main helical conformations in immunogenic formulations based on alum, Freund's adjuvant, or two different types of liposomes. Binding to membrane-inserted MPERp, IR, molecular dynamics simulations, and characterization of the immune responses further suggested that packed helical bundles partially inserted into the lipid bilayer, rather than monomeric helices adsorbed to the membrane interface, could encompass effective MPER peptide vaccines. Together, our data constitute a proof-of-concept to support MPER-based peptides in combination with liposomes as standalone immunogens and suggest new approaches for structure-aided MPER vaccine development.

The envelope (Env)[8] glycoprotein subunits gp120 (surface) and gp41 (transmembrane), which mediate receptor binding and virus-cell fusion, respectively, are organized as trimers of noncovalently associated heterodimers on the surface of the HIV-1-producing cells and assembled virions (1, 2). Upon receptor/co-receptor engagement by gp120, the gp41 ectodomain undergoes a series of conformational changes to deliver the energy required for membrane merger (3–5). The functional Env complex is also targeted by the broadly neutralizing antibodies (bNAbs) known to block infection by a wide range of HIV-1 strains (1, 4, 6). These antibodies are triggered in a

* This work was supported in part by Spanish MINECO Grants BIO2011-29792 (to J. L. N.), BFU2010-22103 (to J. L. R. A.), and CTQ2011-22514 (to M. A. J.) and Basque Government Grants IT838-13 and IT852-13 (to J. L. N. and J. L. R. A., respectively).
[S] This article contains supplemental Tables S1 and S2.
The atomic coordinates and structure factors (codes 2M8M and 2M8O) have been deposited in the Protein Data Bank (http://wwpdb.org/).
[1]H chemical shifts for MPERp in HFIP and DPC were deposited in the BioMagResBank under accession number 19262 and 19263.
[1] Both authors contributed equally to this work.
[2] Recipient of a predoctoral fellowship from Spanish MINECO.
[3] Recipients of predoctoral fellowships from the Basque Government.
[4] Supported by Canadian Institutes for Health Research Grant NRF-126638 and the Canada Research Chairs Program.
[5] Supported in part by the National Science Foundation through Major Research Instrumentation Grant CNS-09-58854.
[6] To whom correspondence may be addressed. Tel.: 34-91-745-9541; E-mail: majimenez@iqfr.csic.es.
[7] To whom correspondence may be addressed. Tel.: 34-94-601-3353; Fax: 34-94-601-3360; E-mail: gbpniesj@lg.ehu.es.

[8] The abbreviations used are: Env, envelope; bNAb, broadly neutralizing antibody; Chol, cholesterol; DPC, dodecylphosphocholine; HFIP, 1,1,1,3,3,3-hexafluoro-2-propanol; MPER, membrane-proximal external region; PA, phosphatidic acid; POPC, 1-palmitoyl-2-oleoylphosphatidylcholine; POPG, 1-palmitoyl-2-oleoylphosphatidylglycerol; TMD, transmembrane domain; PDB, Protein Data Bank; CDR, complementarity-determining region; MDS, molecular dynamics simulation.

fraction of infected individuals only upon prolonged contact with the virus (7, 8). It has been proposed that vaccination strategies focused on the induction of antibodies qualitatively similar to those bNAbs might result in the effective prevention of infection (7, 9).

The isolation of bNAbs in the form of monoclonal antibodies (MAbs) has revealed common structural trends useful for guiding the rational design of immunogens eliciting protective antibodies (9–11). Broad neutralization is attained by antibodies that bind to a handful of invariable but accessible regions of gp120 and gp41. Broadly neutralizing sera raised to gp120 have been found to contain antibodies that target the receptor-binding site, the glycan-V3 site, and the V1V2 loops, whereas antibodies in broadly neutralizing sera raised to gp41 appear to bind exclusively to the "membrane-proximal external region" (MPER) or pre-transmembrane domain within this subunit (7–10, 12, 13).

In contrast to the structurally complex, discontinuous epitopes recognized by anti-gp120 bNAbs, it is hypothesized that MPER embodies a single continuous linear epitope (14–18). Following this idea, it has been suggested that synthetic peptides constrained into the neutralization-competent MPER structures might constitute stand-alone vaccines (19, 20). One anti-MPER bNAb that has focused much attention in this research area is the 2F5 antibody. 2F5 was isolated in mAb form by Katinger and co-workers (21, 22) from a panel of sera from naturally infected asymptomatic individuals. Given the neutralization breath and potency shown by the bNAb 2F5 (13, 21, 23–26), development of peptide-based vaccines targeting the 2F5 epitope has since been pursued (6, 22, 27–33).

Binding specificity of MAb2F5 was initially mapped to N-terminal ^{662}ELDKWA^{667} MPER residues (21, 24, 26). Based on mass spectrometry and proteolytic protection assays, this core epitope was later extended to span the ^{656}NEQELLELDKWASLWN^{671} sequence (34). Comparable full epitope lengths were subsequently suggested by competition ELISA (35) and structural analyses (14, 36). X-ray crystallography further indicated that epitope binding does not involve the hydrophobic apex of the long complementarity-determining region (CDR)-H3 loop, an element shown to be crucial for the neutralizing function of the antibody (37, 38). Given the close proximity of the epitope to the envelope surface, it has been proposed that the 2F5 CDR-H3 loop might interact directly with viral membrane lipids (14, 39–41). Alternatively, data have been recently reported suggesting that the CDR-H3 loop apex may establish additional contacts with MPER C-terminal residues in helical conformation (25, 38). These two options need not be mutually exclusive for bivalent antibodies targeting the 2F5 epitope on the surface of virions. It has been argued that MAb2F5-like antibodies could use a heteroligation strategy (*i.e.* to combine strong binding to gp41 and weak binding to viral membrane) to increase its avidity under conditions existing in the HIV envelope (9).

Here, we provide unprecedented results on the structure and immunogenicity of a peptide spanning the sequence ^{656}NEQELLELDKWASLWNWFNITNWLWYIK^{683}, which includes the complete 2F5 epitope (underlined), the downstream region proposed to establish weak contacts with the CDR-H3 loop of the antibody, and an aromatic-rich block that allows its insertion into the membrane interface (Fig. 1). The NMR data on this peptide, termed MPERp, support the folding of the complete HIV-1 2F5 epitope within a continuous kinked helix.

IR confirmed the preservation of the main helical conformation in adjuvants representing licensed vaccine formulations (*i.e.* aluminum salt and water-in-oil emulsions) and in two different types of liposomes. Because it is predicted that the liposomal MPERs that mimic the 2F5 epitope will be bound by the functional neutralizing antibody, we performed assays to correlate function and binding. Consistent with previous reports (37, 38), cell infection blocking in our in-house assay was dependent on the CDR-H3 loop. 2F5 binding to MPERp in liposomes made of anionic phospholipid and lipid A was also dependent on the CDR-H3 loop, whereas binding to the peptide on the surface of lesser charged Chol-containing vesicles did not require this element.

All tested MPERp vaccines were immunogenic. However, significant amounts of 2F5 epitope-targeting antibodies with the capacity of blocking cell infection were only recovered from sera of rabbits immunized with liposomal vaccines displaying a correlation between 2F5 antibody function and binding, *i.e.* those based on the anionic phospholipid and lipid A. Insights into the structural basis for functional antibody generation could be gained by combining IR and molecular dynamics simulation (MDS) analyses. These data suggest that membrane-inserted helical bundles, rather than monomers adsorbed to the membrane interface, may embody efficient MPER vaccines. Together, our structural and immunogenicity data conform to the prediction that MPER may fold as a single contiguous antigenic determinant, competent in generating a neutralizing response and therefore supporting the application of derived peptides in combination with liposomes as stand-alone vaccines to target the 2F5 epitope.

EXPERIMENTAL PROCEDURES

Materials—MPERp and the 2F5 peptide epitopes used in the immunological studies were synthesized in C-terminal carboxamide form by solid phase methods using Fmoc (*N*-(9-fluorenyl)methoxycarbonyl) chemistry, purified by reverse phase HPLC, and characterized by matrix-assisted time-of-flight (MALDI-TOF) mass spectrometry (purity >95%). Peptides were routinely dissolved in dimethyl sulfoxide (DMSO, spectroscopy grade), and their concentration was determined by the bicinchoninic acid microassay (Pierce). 1-Palmitoyl-2-oleoylphosphatidylglycerol (POPG), 1-palmitoyl-2-oleoylphosphatidylcholine (POPC), phosphatidic acid (PA), Chol, and lipid A detoxified (*Salmonella minnesota* R595) were purchased from Avanti Polar Lipids (Birmingham, AL). Dodecylphosphocholine (DPC) was from Anatrace (Maumee, OH). MAb2F5 was kindly donated by Dietmar Katinger (Polymun Scientific, Klosterneuburg, Austria). Fab2F5-WT and Fab2F5-ΔCDR-H3 were produced as described previously (38).

Recording of NMR Spectra—NMR samples were prepared by dissolving the lyophilized peptides (~1 mg) in 0.5 ml of a H_2O/D_2O (9:1 ratio by volume) solution containing 2 mM HEPES buffer at pH 7.0 and either 25% (v/v) 1,1,1,3,3,3-hexafluoro-2-propanol (HFIP; D2, 98%; Cambridge Isotopes Lab) or 20 mM

TABLE 1
Structural statistics for the ensemble of the 20 lowest energy NMR structures of MPERp in DPC (20 mM deuterated dodecylphosphocholine, 2 mM HEPES, pH 7.0, H_2O/D_2O, 9:1, v/v) and HFIP (25% deuterated 1,1,1,3,3,3-hexafluoro-2-propanol in 2 mM HEPES, pH 7.0, H_2O/D_2O, 9:1, v/v)

		DPC	HFIP
No. of distance restraints	Intraresidue ($i - j = 0$)	154	118
	Sequential ($\|i - j\| = 1$)	103	74
	Medium range ($1 < \|i - j\| < 5$)	115	35
	Total number	372	227
	Averaged total no./residue	13.3	8.0
No. of dihedral angle constraints	ϕ angles	26	26
	ψ angles	25	22
	Total number	51	48
Average maximum violations/structure	Distance (Å)	0.15 ± 0.01	0.02 ± 0.04
	Dihedral angle (°)	3.5 ± 0.1	0.1 ± 0.1
Averaged structure energies	CYANA target function value	0.35 ± 0.01	0.01 ± 0.01
	AMBER energy (kcal/mol)	−1187	−602
	van der Waals energy (kcal/mol)	−195	−182
	Electrostatic energy (kcal/mol)	−2247	−2235
Deviations from ideal geometry	Bond length (Å)	0.014	0.015
	Bond angle (°)	1.8	1.7
Pairwise root mean square deviation (Å) (residues 2–27)	Backbone atoms	0.4 ± 0.4	1.6 ± 0.7
	All heavy atoms	1.1 ± 0.3	2.5 ± 0.7
Ramachandran plot (%)	Residues in most favored regions	99.6	98.8
	Residues in additional allowed regions	0.4	1.2
	Residues in generously allowed regions	0.0	0.0
	Residues in disallowed regions	0.0	0.0

deuterated DPC (D38, 98%; Cambridge Isotopes Lab). Peptide concentrations were ~0.5 mM. pH was measured with a glass microelectrode and not corrected for isotope effects. A methanol sample was used to calibrate the temperature of the NMR probe. Chemical shifts were referenced to internal sodium 2,2-dimethyl-2-silapentane-5-sulfonate.

The ^{1}H NMR spectra were acquired on a Bruker Avance-600 spectrometer operating at a proton frequency of 600.13 MHz and equipped with a cryoprobe. One-dimensional spectra were acquired using 32 K data points, which were zero-filled to 64 K data points before performing the Fourier transformation. Phase-sensitive two-dimensional correlated spectroscopy (COSY), total correlated spectroscopy (TOCSY), and nuclear Overhauser enhancement spectroscopy (NOESY) spectra were recorded by standard techniques using presaturation of the water signal and the time-proportional phase incrementation mode, as reported previously (42). NOESY mixing times were 100 or 150 ms, and TOCSY spectra were recorded using 60 ms DIPSI2 with z filter spin-lock sequence. Acquisition data matrices were defined by 2048 × 512 points in t_2 and t_1, respectively. Data were processed using the standard TOPSPIN program (Bruker Biospin, Karlsruhe, Germany). The two-dimensional data matrix was multiplied by either a square-sine-bell or a sine-bell window function with the corresponding shift optimized for every spectrum and zero-filled to a 2K × 1K complex matrix prior to Fourier transformation. Baseline correction was applied in both dimensions.

Structure Calculation—The same protocol was followed to calculate the structures of MPERp in the presence of DPC micelles and in 25% HFIP from distance and dihedral angle constraints derived from NMR parameters. Distance constraints were obtained from the 150-ms two-dimensional ^{1}H-^{1}H NOESY spectra, with the cross-peaks observed in the 100-ms two-dimensional ^{1}H-^{1}H NOESY being essentially the same. Dihedral angle restraints for ϕ and ψ angles were derived from $^1H_\alpha$ chemical shifts using the program TALOS (43). Structures were calculated using a three-step protocol. First, the standard iterative procedure for automatic NOE assignment of the program CYANA 2.1 (44) was applied. The protocol consists of seven cycles of combined automated NOE assignment and structure calculation of 100 conformers per cycle (45). The list of distance constraints resulting from the last automatic cycle was checked by inspection of the corresponding NOESY spectra, and ambiguous constraints were removed or relaxed to generate the final list used as input for a standard simulated annealing CYANA 2.1 calculation of 100 conformers. The 20 conformers with the lowest target function values were selected and subjected to 2000 steps of energy minimization using the generalized Born continuum solvation model with a nonbonded cutoff of 10 Å as implemented in the program AMBER9 (Case DA, Darden TA, Cheatham III TE, University of California, San Francisco). The structural statistics data for the final ensembles of 20 structures obtained for MPERp are provided in Table 1. The quality of these final structures was assessed using PROCHECK/NMR (46) as implemented at the Protein Structure Validation Suite server. All of the residues were either in the most favored or allowed regions of the Ramachandran map (Table 1). The structural ensembles calculated for MPERp have been deposited in the PDB Data Bank with accession codes 2M8M (HFIP) and 2M8O (DPC). These structures were visualized and examined using the programs MOLMOL (47) and Swiss-Pdb viewer (48).

Membrane Binding Assays—Vesicle flotation experiments in sucrose gradients were performed following the method described by Yethon *et al.* (49). In brief, 100 μl of a sample containing rhodamine-labeled liposomes (3 mM lipid concentration) was adjusted to a sucrose concentration of 1.4 M in a final volume of 300 μl, and subsequently overlaid with 400- and 300-μl layers of 0.8 and 0.5 M sucrose, respectively. The gradient was centrifuged at 436,000 × *g* for 3 h in a TLA 120.2 rotor (Beckman Coulter, Brea CA). After centrifugation, four 250-μl fractions were collected. Material adhered to tubes was collected into a 5th fraction by washing with 250 μl of hot (100 °C) 1% (w/v) SDS.

Infrared Spectroscopy—Infrared spectra were recorded in a Thermo Nicolet 5700 spectrometer equipped with a mercury-

cadmium-telluride detector using a Peltier-based temperature controller (TempCon, BioTools Inc., Wauconda, IL) with calcium fluoride cells (BioCell, BioTools Inc., Wauconda, IL). MPERp-containing samples were lyophilized and subsequently prepared at 4 mg/ml in D_2O buffer (5 mM HEPES, pD 7.4, 100 mM NaCl). A 25-μl sample aliquot was deposited on a cell that was sealed with a second cell. Reference windows without peptide were prepared similarly. Typically 370 scans were collected for each background and sample, and the spectra were obtained with a nominal resolution of 2 cm^{-1}. Data treatment and band decomposition of the original amide I have been described elsewhere (50).

Cell Entry Assays—For the in-house cell entry assays (38), HIV-1 pseudoviruses were produced by transfection of human kidney HEK293T cells with the full-length Env clone JRCSF (kindly provided by Jamie K. Scott and Naveed Gulzar, Simon Fraser University, British Columbia, Canada) using calcium phosphate. Cells were co-transfected with vectors pWXLP-GFP and pCMV8.91, encoding, respectively, a green fluorescent protein and an Env-deficient HIV-1 genome (provided by Patricia Villace, Consejo Superior de Investigaciones Científicas, Madrid, Spain). After 24 h, the medium was replaced with OptiMEM-Glutamax II (Invitrogen) without serum. Two days after transfection, the pseudovirus particles were harvested, passed through 0.45-μm pore sterile filters (Millex® HV, Millipore NV, Brussels, Belgium), and finally concentrated by ultracentrifugation in a sucrose gradient. HIV entry was determined using TZM-bl target cells (AIDS Research and Reference Reagent Program, Division of AIDS, NIAID, National Institutes of Health, contributed by J. Kappes). Antibody samples were set up in duplicate in 96-well plates and incubated for 1 h at 37 °C with a 10–15% tissue culture infectious dose of pseudovirus. After antibody-pseudovirus co-incubation, 10,000 target cells were added in the presence of 15 μg/ml DEAE-dextran (Sigma). Infection levels after 72 h were inferred from the number of GFP-positive cells as determined by flow cytometry using a FACSCalibur flow cytometer (BD Biosciences).

Molecular Dynamics Simulations—Atomic coordinates of the MPER peptide were taken from the NMR structure calculated in DPC micelles (first model). Only gp41 residues 656 to 683 were included in the model, with sequence NEQELLELDKWASLWNWFNITNWLWYIK. Default protonation states were used for all the ionizable residues. N and C termini were amidated and acetylated, respectively.

A pre-equilibrated bilayer containing a mixture of POPC/1-palmitoyl-2-oleoyl phosphatidic acid/Chol in ratios 2:1.5:0.2 and pure POPG in a one-component bilayer were used. The systems were solvated by ~37,000 water molecules. Sodium and chloride ions were added to neutralize the systems up to a final experimental concentration of 150 mM. Four MPER peptides were randomly placed in the solution at the start of the simulations. The total production runs were 235 ns for each simulation. MD trajectories were simulated with the version 2.9 of NAMD (51), using the CHARMM27 force field with CMAP corrections for the peptides (52), the CHARMM36 force field for lipids (53), the TIP3P model for water molecules (54), and the model of Cournia *et al.* (55) for cholesterol. Standard parameters for ions in the CHARMM27 force field were adopted. Simulations were performed in the NpT ensemble. Pressure was kept at 1 atm by the Nose-Hoover Langevin piston method (56, 57) with a damping time constant of 100 ps and a period of 200 ps. Temperature was kept at 300 K by coupling to a Langevin thermostat, with a damping coefficient of 5 ps^{-1} (57). Electrostatic interactions were treated by the Particle Mesh Ewald algorithm, with grid spacing below 1 Å (58). van der Waals interactions were truncated at 12 Å and smoothed at 10 Å. Hydrogen atoms were restrained by the SETTLE algorithm (59), which allowed a 2-fs time step.

Rabbit Immunization and Antibody Purification—For immunization in Freund's adjuvant or alum, MPERp was dissolved in 0.5 ml of PBS and mixed with an equal volume of 1.3% (w/v) aluminum hydroxide (Alhydrogel, Superfos Biosector, Denmark) or Freund's adjuvant (Sigma). Liposome-based formulations were prepared following the methods described by Dreesman *et al.* (60) and Maeso *et al.* (61) and included lipid A as adjuvant (62). MPERp in DMSO was added at a final peptide-to-lipid ratio of 1:50 (mol/mol) to a stirring solution of freeze-thaw POPC/Chol/PA/lipid A (2.0:1.5:0.2:0.01 molar ratio) or POPG/lipid A (3.7:0.01 molar ratio) vesicles dispersed in PBS. After incubation for 30 min, the samples were lyophilized. New Zealand White rabbits were inoculated intradermally at multiple sites on day 0 with 1 ml of sample reconstituted in pure water, which contained 0.5 mg of peptide. For subsequent boosting injections, 1 ml of the reconstituted liposome formulation containing 0.3 mg of peptide was used on day 15 (0.3 mg peptide), and 0.2 mg of liposomal peptide was injected on days 30, 45, and 60. The 2F5 epitope-specific antibodies were recovered from sera through affinity purification. To that end, the 2F5ep-Cys (NEQELLELDKWASLWN-C) peptide was immobilized onto a beaded agarose support using a Sulfolink immobilization kit for peptides (Thermo Scientific, Rockford, IL) and following the manufacturer's instructions. The remaining nonspecific binding sites in columns were blocked adding L-cysteine·HCl at 50 mM. Every analyzed serum was loaded on the columns after diluting and filtering it to remove the particulate material. They were allowed to flow through the columns five times thus allowing the binding of all the antibodies present in the serum that recognize specifically the immobilized peptide. After washing the columns with at least 10 bed volumes of 500 mM NaCl containing buffer to dispose of nonspecifically bound antibodies and serum proteins, the specific antibodies were eluted using 100 mM glycine buffer at pH 2.5. The fraction that is not recovered using acidic pH was eluted using freshly made 100 mM triethylamine buffer at pH 11.5.

RESULTS

Designation of the MPER Peptide Containing the Complete 2F5 Epitope—The diagram displayed in Fig. 1*A* designates MPER as the membrane-proximal sequence that connects the gp41 globular ectodomain (FP-NHR-loop-CHR) with the membrane-spanning domain (TMD). Position for the core epitope recognized by the 2F5 bNAb is also displayed. The organization of this region within the pre-fusion gp41 structure recognized by this antibody is presently unknown. Nonetheless, MPER is postulated to embody a single neutralization-competent structure (19, 20).

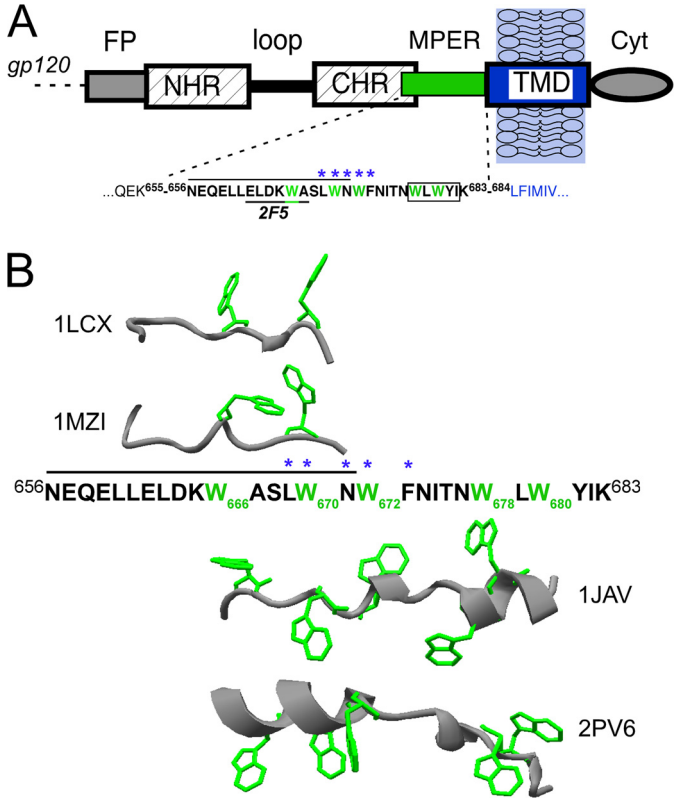

FIGURE 1. **Design of MPER-derived peptide vaccine.** *A,* scheme describing the HIV-1 gp41 organization and the sequence of the MPER peptide vaccine used in this study (HIV-1 Env residues 656–683, numbering and sequence derived from the prototypic HXBc2 isolate). The gp41 ectodomain regions designated in the top diagram include the following abbreviations: *FP,* fusion peptide; *NHR* and *CHR,* N- and C-terminal helical regions, respectively; *Cyt,* cytosolic domain. The MPER sequence below highlights the five Trp residues in green and the core epitope residues recognized by 2F5 antibody *underlined*. The *line* on top spans the extended 2F5 epitope as defined by proteomic analyses (34). *Blue asterisks* denote residues implied in secondary binding by CDR-H3 loop (25) and the *box* an aromatic rich anchor to the membrane interface. *B,* structures adopted by MPER-derived peptides. PDB accession numbers indicated in the panel designate structures in solution (1LCX and 1MZI) or in contact with DPC micelles (1JAV and 2PV6). Lateral side chains of Trp residues are depicted in *green* to align the structures with the MPER amino acid sequence.

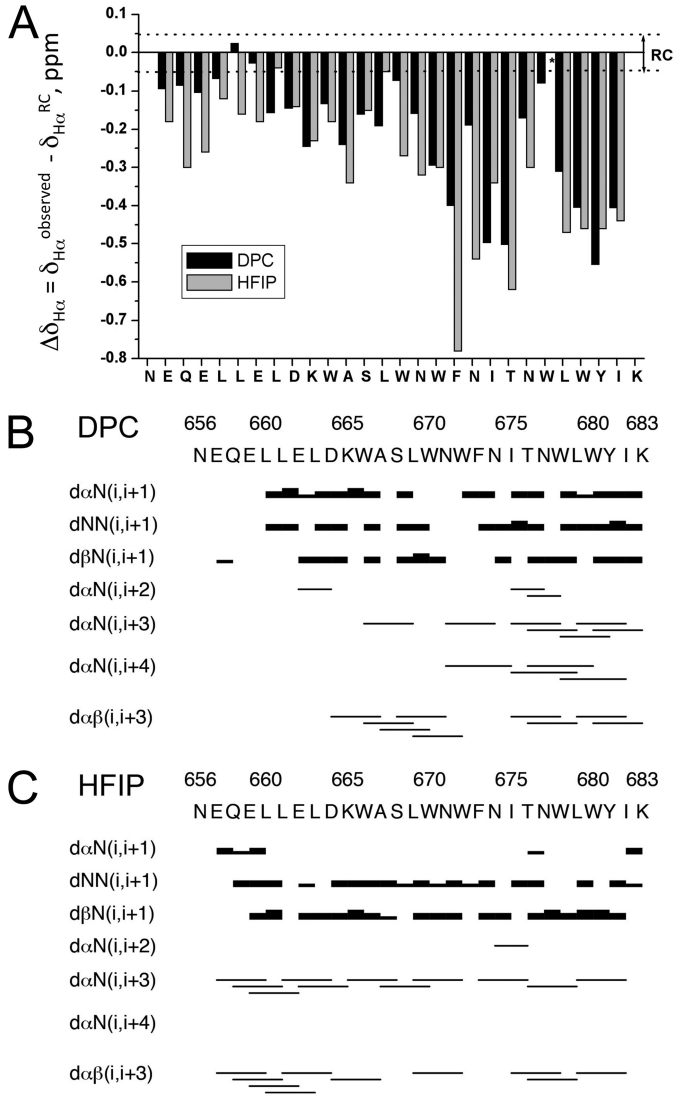

FIGURE 2. **NMR parameters for MPERp.** *A,* bar graphics showing the $\Delta\delta_{H\alpha}$ ($\Delta\delta_{H\alpha} = \delta_{H\alpha}^{observed} - \delta_{H\alpha}^{RC}$, ppm) values as a function of sequence in 20 mM DPC (*black bars*) or 25% HFIP (*gray bars*) at pH 7.0 and 25 °C. *Dashed lines* indicate the random coil (*RC*) ranges. Random coil values for $C_\alpha H$ protons were taken from Wishart *et al.* (66). The N- and C-terminal residues are excluded because of charged end effects. *B* and *C,* NOE summaries for the peptide in 20 mM DPC and 25% HFIP. The intensities of the sequential NOEs, classified as strong, medium, and weak, are indicated by the *thickness* of the *lines*.

Fine definition of the 2F5 epitope suggests the involvement in antibody recognition of a helical stretch that follows the core epitope residues (34, 36, 63). It has been argued that the MAb2F5's CDR-H3 loop establishes contact with residues located further downstream within a continuous helix (25, 38). Because the CDR-H3 loop is absolutely required for the 2F5 neutralizing activity (see below and Ref. 37), it is inferred that those residues constrained into a relevant conformation might be required for peptide vaccines to elicit broadly neutralizing 2F5-like antibodies. The reported three-dimensional NMR structures of MPER peptides are either disconnected from the MPER C-terminal residues (*e.g.* PDB codes 1LCX or 1MZI in Fig. 1*B*) or depleted from the N-terminal 2F5 epitope residues (*e.g.* PDB codes 1JAV or 2PV6 in Fig. 1*B*). Thus, we first attempted the NMR structure resolution of a synthetic peptide vaccine (MPERp, Fig. 1*B*), which included both a complete 2F5 epitope sequence and the C-terminal residues putatively engaged in secondary interactions with the CDR-H3 of MAb2F5 (25, 38).

NMR Solution Structure of MPERp—The ^{1}H NMR signals of MPERp in the presence of DPC micelles and in 25% HFIP at pH 7.0 and 25 °C were assigned by standard sequential assignment methods (64, 65). These chemical shifts have been deposited at BioMagResBank with accession codes BMRB-19263 (DPC) and BMRB-19262 (HFIP). In this peptide, under both conditions, most ^{1}H chemical shifts (supplemental Tables S1 and S2) deviated significantly from random coil values (66). In particular, most H_α protons showed large negative $\Delta\delta_{H\alpha}$ values (Fig. 2*A*). This is a clear indication that MPERp adopted helical structures under both conditions, because according to the well established empirical relationship between the $\Delta\delta_{H\alpha}$ and the ϕ and Ψ as in previous page 3 dihedral angles, positive and negative $\Delta\delta_{H\alpha}$ values are characteristic of β-strands and α-helices, respectively. Additional and stronger evidence for the adoption

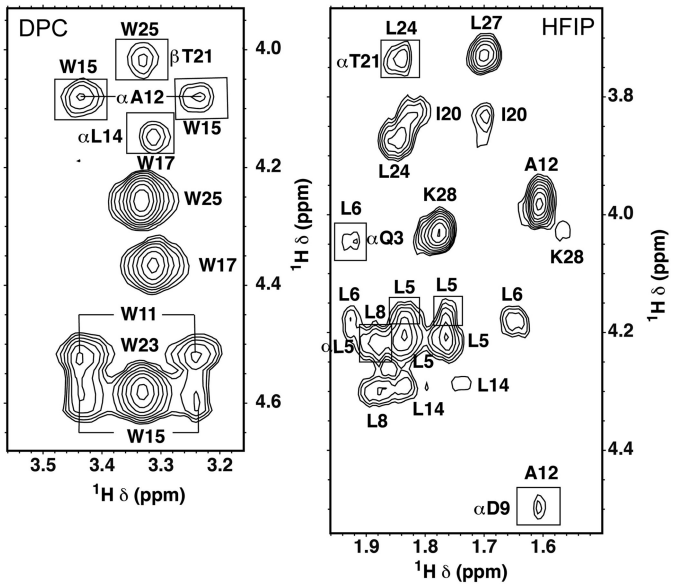

FIGURE 3. **Selected NOESY spectral regions of MPERp in DPC or HFIP conditions (*left* and *right panels*, respectively).** The depicted regions show intraresidue α-β and nonsequential α-β (i, i+3) NOES. The nonsequential NOEs are *boxed*.

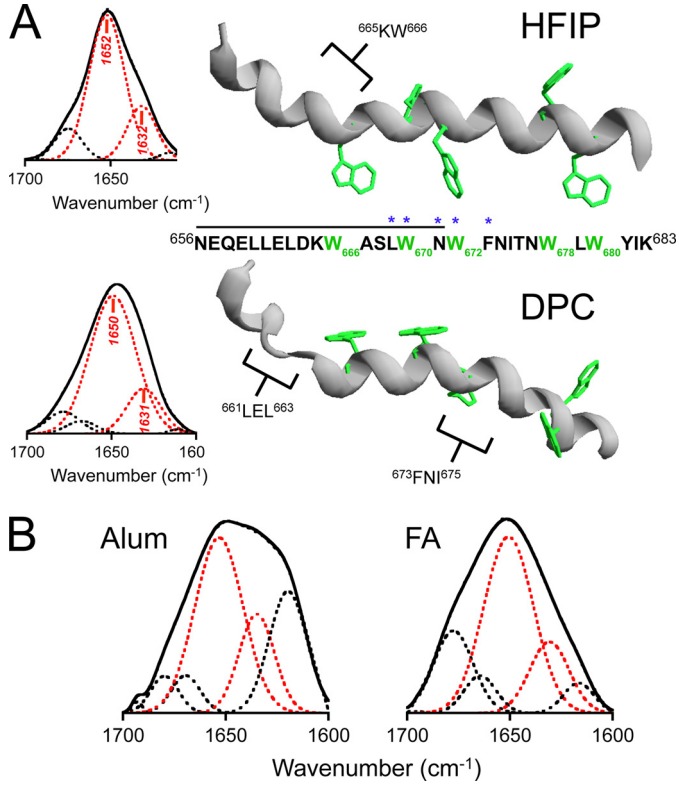

FIGURE 4. **Structures adopted by MPERp in 25% HFIP or DPC 20 mM and classical vaccine adjuvants.** *A,* calculated NMR structures and corresponding IR spectra. Lateral side chains of Trp residues are depicted in *green* and aligned with the amino acid sequence as in the caption for Fig. 1. Both structures are continuous helices. Additional structural signatures common to all calculated models are *highlighted* (see text). The corresponding IR spectra displayed on the *left* disclose in *red* the absorption band components arising from the helical conformation (Table 2). *B,* IR absorption in the amide I region by MPERp in D_2O-based buffer mixed with solutions of alum and Freund's adjuvant (*FA*) following the procedure used for preparing vaccines. In all panels the IR spectra were decomposed into different band components (numerical values are disclosed in Table 3). *Red dotted lines* correspond to α-helix components.

of helical structures in both media came from the set of observed NOEs, because NOE cross-peaks are only observed for pairs of spatially closed protons (approximately at a distance less than 5 Å). The nonsequential NOEs presented by the peptide were those characteristic of helices, *i.e.* $d_{\alpha N(i+2)}$, $d_{\alpha N(i+3)}$, $d_{\alpha N(i+4)}$, and $d_{\alpha\beta(i+3)}$ (Fig. 2, *B* and *C*). Some of these medium range NOEs can be observed in the NOESY spectral regions shown in Fig. 3.

Structure calculations were further performed to visualize the features of the structure adopted by MPERp in the presence of DPC or when dissolved in 25% HFIP (see under "Experimental Procedures"). In contrast to the structures displayed in Fig. 1*B*, the structures resolved for MPERp disclosed continuous and well defined helical structures in both media (Fig. 4*A*). Although uninterrupted, in both cases the complete set of models showed changes in the direction of the helix axis at certain points. In HFIP, the helix was bent at position ^{665}KW^{666} forming an angle of ~40° (Fig. 4*A*, *top*). More conspicuous changes could be observed in the presence of DPC (Fig. 4*A*, *bottom*). In all calculated DPC structures, the N-terminal residues ^{661}LEL^{663} formed a short 3_{10}-helix, and the following main α-helix bent forming an angle of ~30° at the ^{673}FNI^{675} tripeptide.

IR Structure of MPERp in Classical Adjuvants—High resolution NMR spectroscopy supports the folding of the 2F5 epitope within a continuous MPER helical structure. To determine whether this structure was preserved in vaccine formulations, we measured MPERp conformations in different adjuvants by IR spectroscopy. The reference spectra obtained under the NMR conditions (Fig. 4*A*, *left panels*) showed the absorption of the amide-I centered at ~1650 cm^{-1}, consistent with the α-helix conformation adopted by MPERp in HFIP and DPC mixtures (50). Band decomposition disclosed in both cases an additional low frequency band centered at ~1630 cm^{-1}, corresponding to the solvent-exposed α-helix fraction (67–69). In conjunction, both bands accounted for ~ 85% of the total absorption (red-dotted band components). The analysis also revealed less significant contributions by bands in the 1680- to 1660-cm^{-1} region, indicative of additional fractions of β-turn/3_{10}-helix plus less defined coil structures (Table 2).

Subsequently, we assessed the conformational changes undergone by MPERp in vaccines formulated with aluminum hydroxide (alum) and water-in-oil dispersions (incomplete Freund's adjuvant), which provided two viscous media relevant for the adjuvants currently used in vaccination protocols (70). Consistent with preservation of the main α-helical conformation in these adjuvants, the IR amide-I band maximum was located at ~1650 cm^{-1} in both cases (Fig. 4*B*). However, as compared with DPC or HFIP samples, the peptide dispersed in alum displayed an additional band component centered at 1620 cm^{-1}, indicative of significant denaturation-aggregation evolving in these samples (Table 3). In the inverted micelle medium provided by Freund's adjuvant, the band was broader than in DPC or HFIP, and its decomposition revealed that β-turn, 3_{10}-helix, and less ordered conformers absorbing in the 1680–1660 cm^{-1} region were comparatively more abundant than in the NMR references (Table 3).

2F5 Binding to Liposomal Vaccines—In addition to the standard adjuvants, MPERp was combined with liposomes to compose synthetic vaccines. It has been suggested that interactions with the membrane interface on the surface of liposomes may select for the MPER conformations that are relevant for the induction of specific antibodies (62), whereas polyreactivity with membrane lipids could increase the binding avidity of those antibodies (9). For this study, we selected two different lipid compositions. In one formulation MPERp was administered together with POPC/Chol/PA (2:1.5:0.2 mol/mol) liposomes, and in a second formulation the peptide was combined with vesicles made of the anionic phospholipid POPG. It is assumed that peptide structures relevant for the 2F5 epitope will be bound by the functional 2F5 antibody but not by their inactive mutants. Thus, to discriminate functional *versus* nonfunctional binding, we used CDR-H3 mutant Fabs that bind peptide epitopes in solution but are not neutralizing (Fig. 5).

Fig. 5*A* compares the capacity for inhibiting viral entry of the MAb2F5 and two derived Fabs, Fab2F5-WT and Fab2F5-ΔCDR-H3, with the latter representing a mutant with the CDR-H3 loop deleted (38). MAb2F5 and Fab2F5-WT inhibited pseudovirus cell infection in our assay (Fig. 5*A, black* and *blue symbols*, respectively), whereas Fab2F5-ΔCDR-H3 had no effect (*red symbols*). To determine a functional correlation with epitope binding, we next compared the capacity of these antibodies to bind the liposomal vaccines (Fig. 5, *B–E*). Experiments were set up for obtaining pure vesicles floating on the top fractions of sucrose gradients (Fig. 5*B*). These assays indicated quantitative MPERp incorporation into the POPC/Chol/PA and POPG liposomes (Fig. 5*C*). Results displayed in Fig. 5*D* further demonstrated that MAb2F5 could effectively bind to the membrane-inserted peptide epitopes in both types of liposomes. Thus, according to this sole criterion, both types of vesicles containing peptide might encompass effective 2F5 immunogens. However, the comparison of the Fabs revealed different patterns (Fig. 5*D*). The functional Fab2F5-WT reproduced the binding pattern of the mAb (Fig. 5*D, top*). In contrast, the nonfunctional Fab2F5-ΔCDR-H3 could bind effectively to POPC/Chol/PA-MPERp liposomes but not to POPG-MPERp liposomes (Fig. 5*D, bottom*).

Thus, cell entry inhibition and binding to POPG-MPERp liposomes were both dependent on the CDR-H3 loop. Together, these results allowed establishing a correlation between function and binding to POPG-bound MPERp, which was not found for the POPC/Chol/PA-MPERp liposomes. Accordingly, we inferred that when used as immunogens POPG-MPERp vaccines would be more selective than POPC/Chol/PA-MPERp vaccines in activating 2F5-like B-cell receptors.

MPERp Structure in Liposomal Vaccines—To gain insights into the membrane-associated structures at the origin of the function-binding correlation, we carried out a combined infrared spectroscopy-molecular dynamics simulation study (Fig. 6). Samples of MPERp in contact with POPC/Chol/PA liposomes closely reproduced the IR absorption spectrum measured in the Freund samples (Fig. 6*A*, *left*). This finding is consistent with the comparable structures adopted by membrane-binding peptides at interfaces of reverse micelles and membranes (71). In sharp contrast, the amide-I band measured in the POPG-MPERp samples was narrower, suggestive of higher conformational order, and corresponded almost exclusively to α-helical conformers (Fig. 6*B*, *left*). In these samples, the maximum shift of the low frequency α-helix band and its increase in intensity were consistent with the existence of packing interactions between solvated helices (67, 68).

Further insights into the membrane-associated structures causing these spectral differences were obtained from the dynamics of the MPERp DPC structure simulated in the presence of POPC/Chol/PA and POPG lipid bilayers (Fig. 6, *right panels*). MPERp was observed to associate as a single monomer with the POPC/Chol/PA membrane (Fig. 6*A*, *right*). In the course of the simulation, this peptide monomer was observed to contact first with the membrane surface through the hydrophobic C-terminal side, and the amphipathic N terminus was inserted later. At the end of the simulation (235 ns), the peptide adopted a continuous helix, whose main axis was parallel to the lipid bilayer plane. In this state, the membrane interface-embedded side chains made contact preferentially with the polar headgroups of POPC, but not with Chol or PA. In addition, 2F5

TABLE 2
Band position, assignment, and % area of the components obtained after curve-fitting of IR spectra displayed in Fig. 4*A*

HFIP		DPC	
Band position[a]	Area[b]	Band position[a]	Area[b]
	%		%
1675 (β-Turns/3_{10}-helix)	11	1678/1665 (β-Turns/3_{10}-helix)	14
1652 (α-helix-buried)	66	1650 (α-Helix-buried)	66
1632 (α-helix-solvated)	20	1630 (α-Helix-solvated)	19
1615 (aggregation)	2	1611 (aggregation)	1

[a] Wave numbers in cm^{-1}. The conformation assigned for each position is indicated below (50, 68).
[b] The values have been rounded off to the nearest integer.

TABLE 3
Band position, assignment, and % area of the components obtained after curve-fitting of IR spectra displayed in Figs. 4*B* and 6, *A* and *B*

Alum		Freund's adjuvant		POPC/Chol/PA		POPG	
Band position[a]	Area (%)[b]	Band position[a]	Area (%)[b]	Band position[a]	Area (%)[b]	Band position[a]	Area (%)[b]
1680/1669 (β-Turns/3_{10}-helix)	11	1678/1665 (β-Turns/3_{10}-helix)	26	1685/1671 (β-Turns/3_{10}-helix)	26	1665 (3_{10}-Helix)	3
1653 (α-Helix-buried)	45	1651 (α-Helix-buried)	52	1652 (α-Helix-buried)	46	1654 (α-Helix-buried)	52
1635 (α-Helix-solvated)	19	1631 (α-Helix-solvated)	17	1637 (α-Helix-solvated)	13	1639 (α-Helix-solvated)	39
1620/1693 (Aggregation)	25	1617 (Aggregation)	5	1615/1627/1686 (Aggregation)	15	1628 (Aggregation)	5

[a] Wave numbers are in cm^{-1}. The conformation assigned for each position is indicated below (50, 68).
[b] The values have been rounded off to the nearest integer.

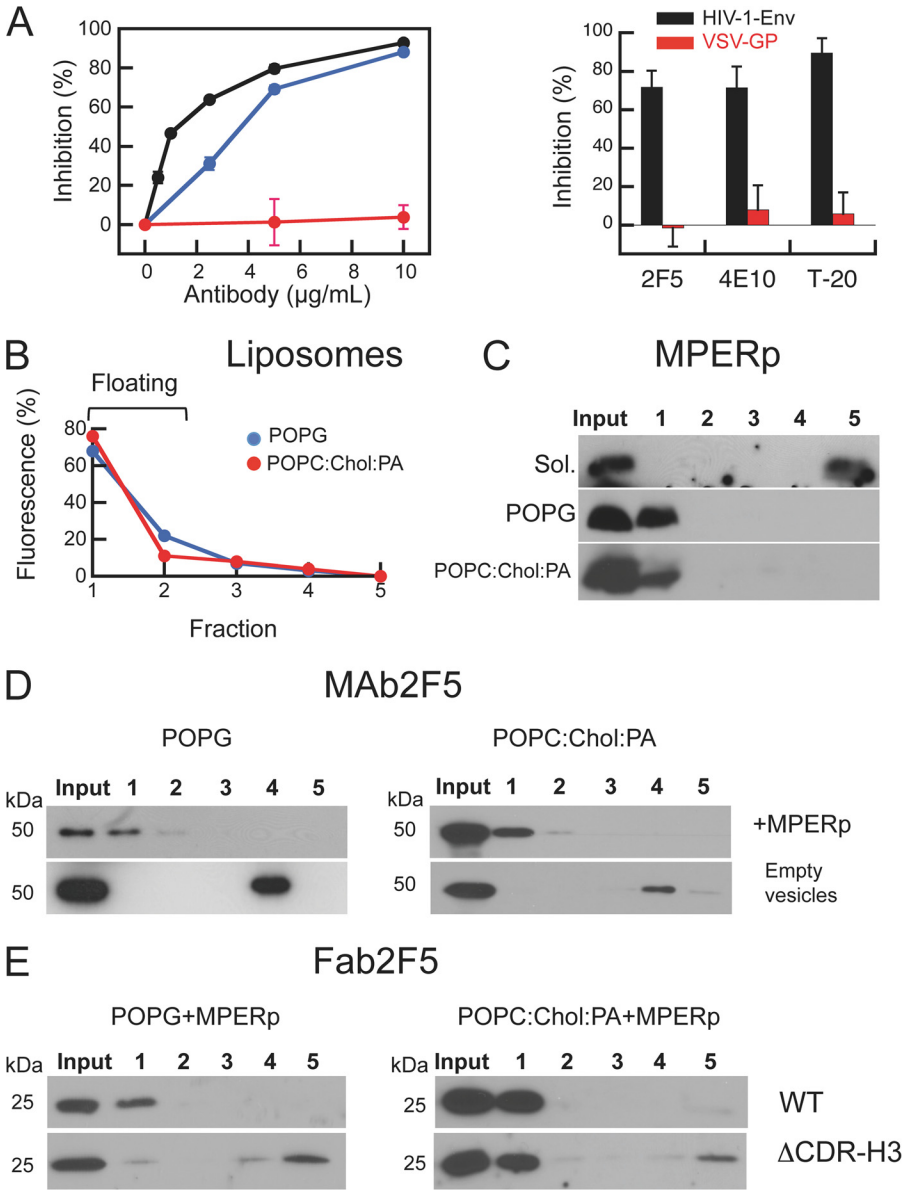

FIGURE 5. **Correlation between 2F5 antibody function and binding to liposomal vaccines.** *A,* cell entry inhibition assay. *Left,* pseudoviruses were preincubated with MAb2F5 or the recombinant 2F5 Fab constructs, and single cell entry events were monitored by FACS after incubation with TZM-bl target cells. Fab2F5 WT inhibited cell entry (*blue*), albeit with lower potency than the bi-functional mAb (*black*). In contrast Fab2F5 ΔCDR-H3 was almost completely unable to inhibit the process (*red*). *Right,* displays specificity controls for the HIV-1 Env-mediated cell entry. bNAbs (2F5 and 4E10) and T-20 were applied at 2 and 50 μg/ml, respectively. Means ± S.D. of six measurements in three independent experiments are displayed. *B–E,* vesicle flotation experiments in sucrose gradients. Rhodamine-labeled liposomes were collected in the 1st and 2nd fractions (*i.e.* floating fractions) (*B*). *C,* MPERp (30 μM) was incubated in solution in absence (*top*) or presence of liposomes (peptide-to-lipid ratio of 1:100, *bottom panels*) for 15 min before centrifugation. The presence of the peptide in the different fractions was probed with MAb2F5 in Western blot. Virtually all input peptide co-floated with liposomes indicating quantitative partitioning into membranes. *D,* MAb2F5 (15 μg ml^{-1}) was incubated for 15 min with MPERp-containing or empty liposomes before centrifugation (*top* and *bottom panels*, respectively). Consistent with antibody binding to membrane-inserted MPERp, MAb2F5 was recovered from the floating fractions upon incubation with peptide-containing liposomes. Similarly, Fab2F5 WT co-floated with both types of MPERp-containing liposomes (*E, top panels*). In contrast, in the case of POPG-MPERp vesicles, Fab2F5 ΔCDR-H3 was predominantly recovered from pellets (*E, bottom panels*).

epitope key residues Lys-665 and Trp-666 (Fig. 6*A*, *red side chains*), as well as residues establishing putative contacts with the CDR-H3 loop (*i.e.* Leu-669, Trp-672, and Phe-673) (*blue side chains*) were involved in these lipid interactions and therefore not accessible from the water solution.

In contrast, the four peptides, randomly placed in solution at the beginning of the simulation, were found assembled into a bundle at 194 ns. This bundle of peptides was associated with the POPG bilayer (Fig. 6*B*, *right*) from 194 ns until the end of the simulation (235 ns). The MPERp bundle inserted through the aromatic rich C-terminal hydrophobic tip of one of the constituent monomers (Fig. 6*B*, residues in *green*) during the simulation. In the course of the simulation, distinct MPERp ensembles retaining overall helical conformation were observed several times to stick in the membrane by the action of a monomer; however, insertion of single peptides was not observed. Moreover, the more polar N terminus of the membrane-inserted monomer never contacted the negatively charged membrane surface. In the membrane-inserted state, residues involved in MAb2F5 recognition (Lys-665, Trp-666, Leu-669, Trp-672, and Phe-673 (see below and Refs. 25,

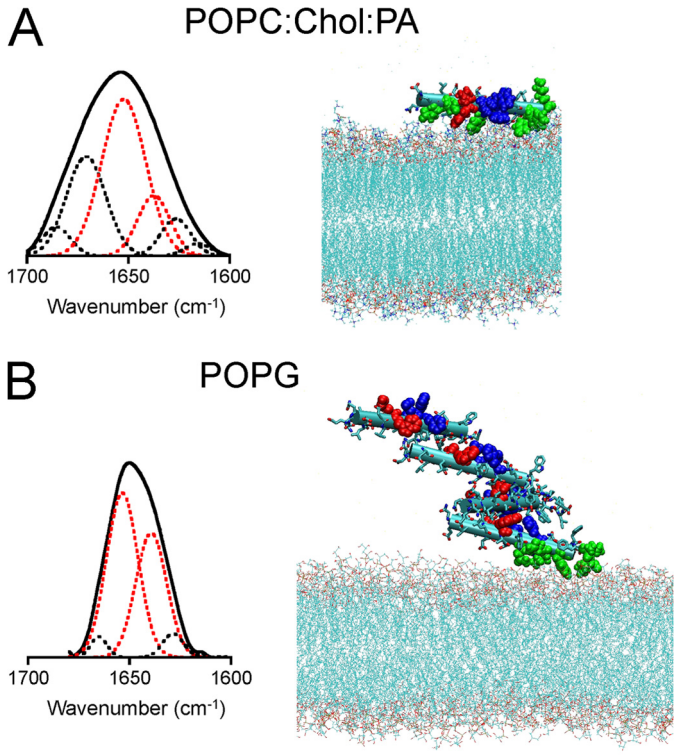

FIGURE 6. **Combined IR and molecular dynamics simulations of MPERp interacting with POPC/Chol/PA (*A*) or POPG (*B*) lipid bilayers.** *Left panels,* IR absorption in the amide I region by MPERp in D_2O-based buffer mixed with solutions of POPC/Chol/PA (2:1.5:0.2 mol/mol) liposomes or POPG liposomes, following the procedure used for preparing vaccines. In both panels, the IR spectra were decomposed into different band components (numerical values are disclosed in Table 3). *Red dotted lines* correspond to α-helix components. *Right panels,* snapshots of MPERp were taken at times 215 and 233 ns (*top* and *bottom,* respectively). Side views of the peptides display in space-filling representation residues Lys-665/Trp-666 in *red* and Leu-669/Trp-672/Phe-673 in *blue*. Phospholipids are shown in *stick* representation. Residues depicted in *green* have at least one atom within <3 Å from the phospholipid molecules.

36, 63) were all exposed to the solution. Nonetheless, the overall shape of the peptide ensemble restricted their accessibility from solvent in some of the monomers.

Immunogenicity of MPERp in the Different Adjuvants—To determine the immunogenicity of the structures described above, the MPERp-based alum, Freund's adjuvant, and liposome formulations were next compared in their capacity for activating B-cell responses (Fig. 7). Antigen-specific IgGs could be recovered upon immunization of rabbits with MPERp dispersed in alum or Freund's adjuvants (Fig. 7*A*, *left* and *left-center panels*). The midpoint titers in these samples were on the order of 10^3. The responses triggered by the peptide-liposome formulations were weaker by comparison, showing midpoint titers in the order of 10^2 (Fig. 7*A*, *right-center* and *right panels*). Nonetheless, antibodies raised against the 2F5 epitope could be recovered from all sera through binding affinity (Fig. 7*B*). Supporting the same range of affinity, incubation in solution of the purified antibodies with 2F5 peptide epitope inhibited with comparable potencies their binding to MPERp deposited on plates (IC_{50} values in the order of 10 μM in all cases). In contrast, the experiments displayed in Fig. 7*C* indicated that the 2F5-targeting antibodies raised by the different formulations were qualitatively different. Those experiments revealed that the only detectable inhibition of HIV entry occurred with the POPG/lipid A-MPERp formulation (Fig. 7*C, right-hand panel*). Of note, blocking VSV-GP-mediated cell infection was not observed in these experiments, which underscores the specificity of the recovered antibodies.

The inhibitory activity of these antibodies was nonetheless ~50–100 times lower than that displayed by the MAb2F5 in the cell entry assays (Fig. 5*A*). Thus, to establish the significance of this activity, we extended our studies on the immunogenicity of the POPG/lipid A-MPERp formulation (Fig. 8). Fig. 8*A* compares midpoint titers and cell entry inhibition by the 2F5-specific antibodies isolated from the sera of four different rabbits. These two values did not correlate, thereby suggesting that even if the immunogenicity levels were different, antibodies were functional in the cell entry assay after isolation in affinity columns. Two groups of sera, R2/R3 and R1/R4, were established as a function of the inhibitory strength of the isolated antibodies (Fig. 8*B*). For the two groups, the inhibition levels of HIV-Env-mediated cell entry were significantly higher than those in the VSV-GP controls. Thus, according to our data in Figs. 7 and 8, we may conclude that antibody samples recovered from POPG sera bore an inhibitory activity of cell entry that was not found in the samples recovered from alum, Freund's adjuvant, or POPC/Chol/PA sera.

DISCUSSION

It has been hypothesized that the membrane-proximal sequence connecting the gp41 subunit's ectodomain with the transmembrane anchor, termed the MPER domain, includes a continuous epitope. This implies that peptides recreating its native structure might in principle compose stand-alone HIV vaccines (6, 13, 19, 20, 72, 73). Although intensively studied, data supporting the structural MPER connectivity within a synthetic peptide vaccine were lacking. Here, we considered the incorporation within a single peptide of the sequence ^{656}NEQELLELDKWASLWN^{671} spanning the full epitope recognized by the MAb2F5 as defined by proteomic analyses, competition ELISA, and crystallography (14, 34–36), plus the following ^{672}WFNITNWLWYIK^{683} Trp-rich stretch that precedes the TMD (Fig. 1) (74). Our NMR data revealed the structuring of the resulting MPERp synthetic surrogate as a continuous helical structure (Figs. 2–4*A*). Structures of shorter or even longer peptides show spots of partial structuring as 3_{10}-and α-helix (33, 35, 73, 75–77), but none of them display continuous helical structures for the sequence spanning the full 2F5 epitope plus the downstream aromatic rich sequence preceding the TMD anchor (Fig. 1). This suggests that inclusion of the complete sequence covered by the 2F5 paratope (34) might be required for the long range interactions sustaining MPER folding as a continuous helix.

Although continuously helical, MPERp NMR structures solved in HFIP and DPC showed features implying a certain degree of conformational flexibility. The kink adopted by the ^{675}FNI^{677} residues at the C terminus of the DPC structure was consistent with the ^{673}FN^{674} hinge described previously for a shorter peptide (73). By comparison, the hinge of the shorter peptide induced a more abrupt change in backbone main direction and adopted a looser conformation (PDB code 2PV6, Fig.

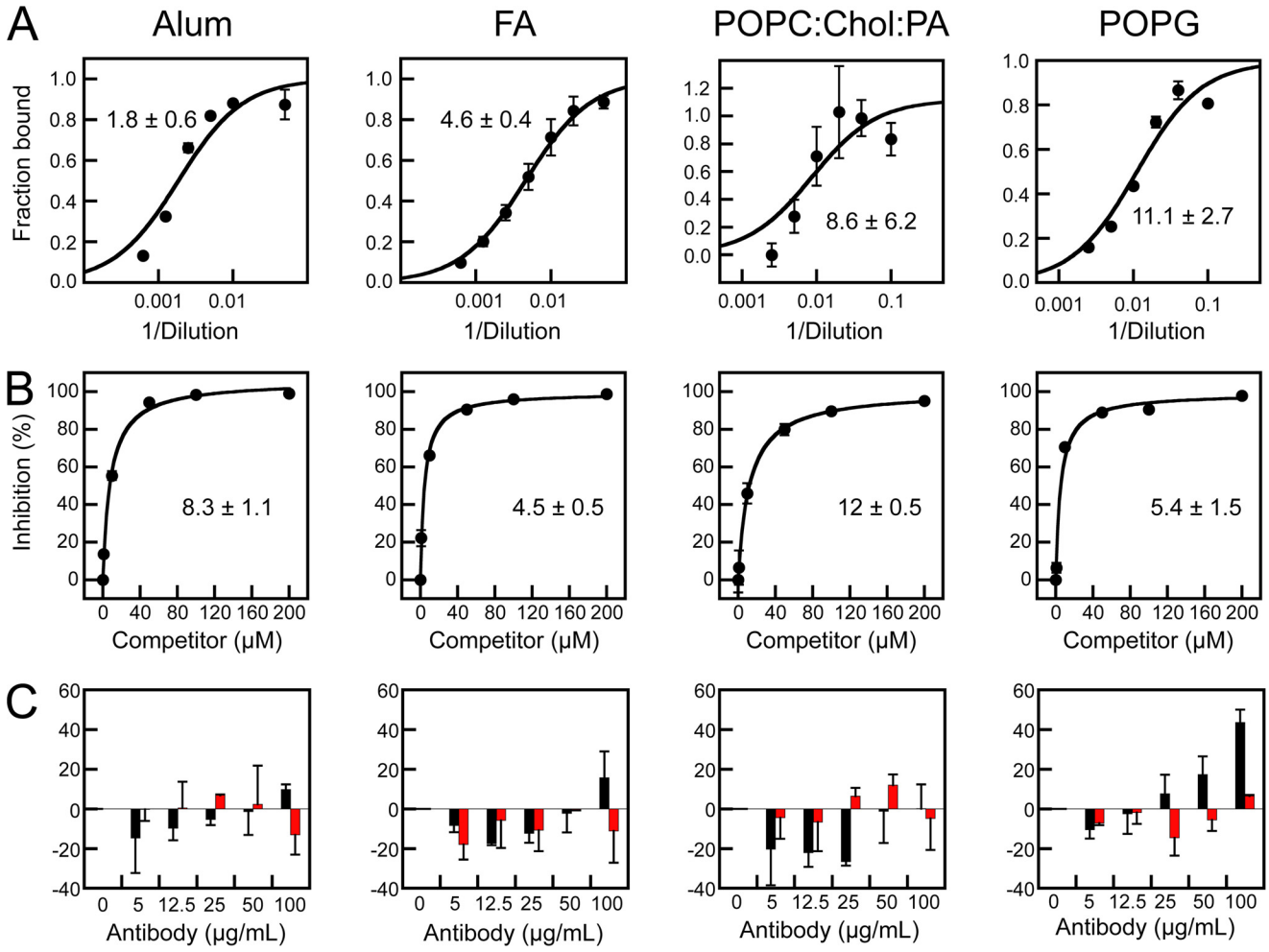

FIGURE 7. **Immunogenicity of MPERp formulated with different adjuvants.** *A,* midpoint IgG titers in sera from rabbits immunized with MPERp in the different adjuvants. Sera were titrated in ELISA using 1.4 μM MPERp. Experimental values were adjusted to sigmoid dose-response curves, and midpoint titers were determined as EC_{50} values (*i.e.* the dilutions giving 50% response between minimum and maximum). Values displayed in panels correspond to 1/dilution $\times 10^3 \pm$ S.E. *B,* affinity for the 2F5 epitope of rabbit IgG purified from sera with 2F5ep-Cys (NEQELLELDKWASLWN-C) peptide immobilized onto a beaded agarose support. Competitive ELISAs were performed using plates coated with MPERp (1.4 μM). Prior to adding to the plates, 0.1 μg/ml of 2F5-specific IgG was preincubated for 30 min with serial dilutions of soluble 2F5ep (NEQELLELDKWASLWN) peptide. Percentages of binding inhibition were adjusted to saturation curves, which were subsequently used to infer the IC_{50} values $\pm$S.E. displayed in the panels. *C,* inhibition of cell entry. In these assays HIV-Env pseudoviruses were preincubated with increasing amounts of purified antibodies, and infection of TZM-bl target cells was subsequently monitored by flow cytometry as in Fig. 5*A*. Plotted inhibition percentage values are means of four experimental determinations. The *red columns* correspond to the level of neutralization exerted on VSV-G-pseudotyped viruses used as negative control.

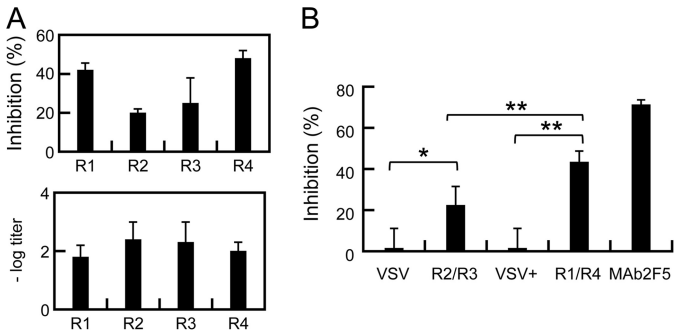

FIGURE 8. **Recovered responses after vaccination with the POPG/lipid A-MPERp formulation.** *A,* midpoint IgG titers (negative log EC_{50} dilution values) and inhibition of cell entry by 2F5-specific antibodies in the sera of four different rabbits (*R1–R4*). Antibodies purified with 2F5ep-Cys were used at 100 μg/ml in the latter assay. *B,* levels of inhibition of cell entry mediated by HIV-1-Env or VSV-GP controls. Rabbits were classified in two groups according to significant differences in the levels of inhibition (R1/R4 *versus* R2/R3). Significant inhibition of Env-HIV-1 *versus* VSV-GP was nonetheless observed for both groups (**, $p < 0.005$; *, $p < 0.05$). MAb2F5 (2 μg/ml) was included as positive control. Means $\pm$ S.D. of six determinations are shown.

1*B*). Thus, the finding that these residues may also exist as part of an elongated α-helix (HFIP structure, Fig. 4*A*) or form a kink while retaining conformational features of an α-helix (DPC structure, Fig. 4*A*), underscores the structural metastability proposed for this joint sequence (73).

Unprecedented structures were additionally observed at the MPERp N-terminal stretch. The HFIP structure displayed a kink involving the ^{665}KW^{666} residues, while the DPC structure displayed a 3_{10}-helix for the ^{661}LEL^{663} residues, which also resulted in a change of the backbone direction (Fig. 4*A*). The presence of these structures would be consistent with the flexibility found in the case of shorter peptides (35). Moreover, they would be consistent with the type I β-turn adopted by the ^{664}DKW^{666} core epitope sequence in Fab2F5-peptide complexes (14, 36, 78). In contrast, our NMR structures did not display the extended conformation found in the crystal structures of those complexes for the preceding N-terminal residues ^{656}NEQELLEL^{663} (14, 36). In both NMR structures

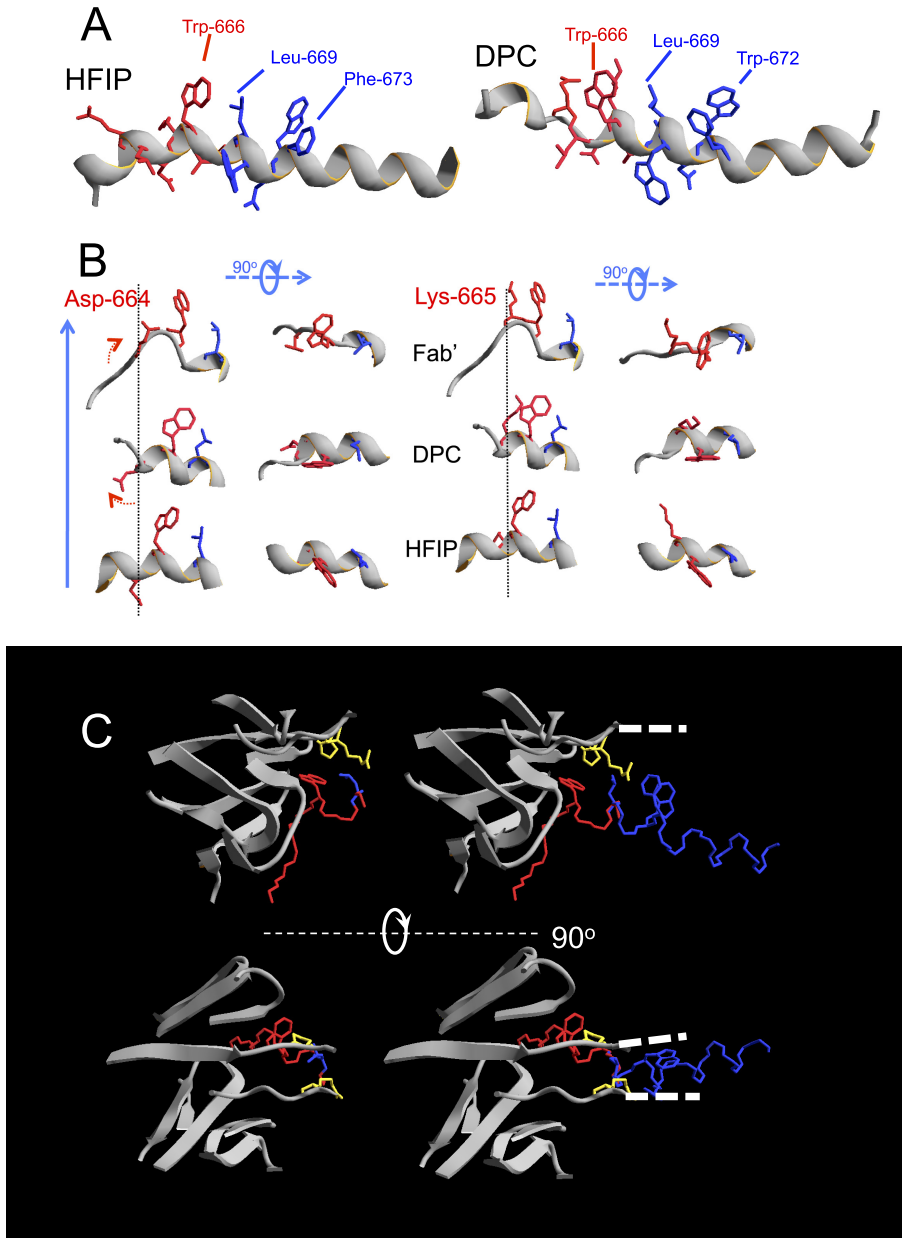

FIGURE 9. **2F5 epitope organization in MPERp and putative mechanism of antibody recognition.** *A,* 2F5 epitope in HFIP and DPC structures. Core epitope residues ELDKWA are shown in *red*, and downstream residues putatively implied in secondary interactions with CDR-H3 loop are depicted in *blue*. Trp-666 and Leu-669/Trp-672/Phe-673 are displayed on the same side of the helix. *B,* comparison of 2F5 epitope structure in Fab' complex (PDB code 3D0L) and MPERp. The chain portion spanning residues Leu-661–Trp-670 is shown in *gray* in the three structures, with projecting side chains of Asp-664 (*left*) or Lys-665 (*right*) and Trp-666 in *red*. Side chain of Leu-669 is displayed in *blue* to establish the relative position of the downstream helix. The comparison suggests that the 3_{10}-helix observed in DPC might include an intermediate of the conformational change required for positioning Asp-664 side chain into the 2F5 paratope. Lys-665 accommodation into the paratope would not require by comparison major conformational changes of the peptide backbone. *C,* fitting of the MPERp helix into Fab'-bound peptide. The Fab paratope structure (PDB code 3D0L) is displayed in *ribbon* representation. The base of the flexible loop of the heavy chain (not solved in the crystal) is marked by the *yellow* side chains of residues Pro-98 and Arg-100B. The MPER residues Trp-666 and Leu-669 in the bound peptide are displayed in *red* and *blue*, respectively. In the *right panel*, the helix turn of MPERp (DPC structure) containing Leu-669 (displayed in blue) has been fitted into the Fab-bound structure. The *dotted lines* mark the estimated position of the loop relative to the MPERp helix.

reported here, these residues rather adopted a helical conformation (Fig. 4*A*).

Even though one should be cautious in interpreting a peptide's conformational states and extrapolating back to the native functional protein, the potential relevance of the helical conformation adopted by MPERp N-terminal residues is emphasized by the structure of an antigenically near-native Env construct termed "SOSIP" gp140 (79). Although truncated at position 664, the recently solved crystal structure at 4.7 Å provides insights into the gp41 ectodomain organization in the context of cleaved, stabilized HIV-1 Env trimers (80). The SOSIP structure supports the location of the ^{656}NEQELLEL^{663} residues into a solvent-exposed helix within the native Env structure.

One crystallographic structure of the 2F5 Fab complexed with peptide further displayed the turn sequence ^{664}DKW^{666} followed by residues ^{667}ASLW^{670} adopting a canonical α-helix conformation (36), which is also present in our NMR structures

(Fig. 4*A*, see also Fig. 9*C*). Thus, in combination, the structural evidence suggests that the native structure recognized by the 2F5 antibody might consist of a continuous helical structure interrupted by a flexible kink at positions 664–666 that redirects the gp41 backbone at the pre-transmembrane region.

Implications for 2F5 Epitope Recognition Mechanism—The MPERp NMR structures solved in this work recreate kinked helical motifs (Fig. 9*A*), which, in combination with previously reported structures (Fig. 9*B*), sustain proposals that this region has evolved to sample alternative conformations after activation of the fusion cascade (25). Within this context, a putative mechanism for 2F5 epitope recognition is presented in Fig. 9*B*. The figure displays the orientations adopted by the ^{664}DKW^{666} residues in MPERp structures and the Fab-bound peptide. The Trp-666 and Leu-669 side chains are oriented in parallel in the three structures, while the negative charge of Asp-664 side-chain projects from the main axis in different directions (Fig. 9*B, left*). By contrast, the alkyl-π stacking between Lys-665 and Trp-666 side chains found in contact with Fab could be fairly reproduced by the structure solved in the DPC structure (Fig. 9*B, right*). In the HFIP structure, further rotation of the Lys-665 side chain would allow its insertion into the Fab binding pocket, without requiring major changes of the peptide backbone conformation. Thus, the NMR structures suggest that binding to a helical MPER peptide might first involve contacting Lys-665, Trp-666, and Leu-669 residues and then require induction by the antibody of a conformational transition in the C_α chain for inserting Asp-664 into the binding pocket. Comparison of the three structures further suggests that the short 3_{10}-helix found in the DPC structure may encompass an intermediate between the fully helical and the extended conformations observed in HFIP- and Fab-bound structures, respectively.

The NMR structures described in this work may in addition provide insights into secondary interactions of the 2F5 antibody with MPER residues C-terminal to the core epitope (Fig. 9*C*). Screening of phage-displayed peptide libraries with the MAb2F5 identified Leu-669 as an almost invariant residue at the C terminus of the core epitope (63). Further competition ELISA demonstrated that the CDR-H3 loop increased binding affinity when C-terminal ^{672}WFNITNWLWYIK^{683} residues were added to the full ^{656}NEQELLELDKWASLWN^{681} epitope sequence (38). This finding raised the possibility that the neutralization dependence on the loop apex was caused by weaker secondary binding to C-terminal MPER residues (38).

Recently reported compelling mutagenesis of the CDR-H3 loop by Güenaga and Wyatt (25) supports that idea. A significant correlation was found between neutralization potency of CDR-H3 mutants and affinity to an MPER peptide spanning residues ^{657}EQELLELDKWASLWNWFNITNWLWYIK^{683}. This correlation was lost in the case of the ^{659}ELLELDKWASL^{669} sequence structurally constrained into a protein scaffold (30). Moreover, L669A, W670A, N671A, W672A, and F673A substitutions, in residues immediately C-terminal to the core epitope, resulted in an affinity decrease. It was further proposed that weak contacts involving π stacking interactions among aromatic residues present in the antibody CDR-H3 loop and the MPER peptide sequence might be responsible for this effect (25). According to these authors, this mode of recognition would in addition enable 2F5 epitope binding when MPER organizes as a helical bundle.

The MPERp structures solved in this work, displaying the relative positions of the 2F5 core epitope and the downstream residues encompassing this secondary antibody-binding site, substantiate such a hypothesis (Fig. 9*C*). Fitting of the MPERp DPC helix ^{667}ASLW^{670} stretch into the corresponding Fab-bound structure (36) disclosed the Leu-669 side chain at the base of the CDR-H3 loop in remarkably similar orientation and aligned the MPER helix axis with the parts of the loops visible in the crystal structure. Thus, the model that emerges from combining both structures supports the possibility that the tip of the CDR-H3 loop may establish contacts with Trp-672 and Phe-673 residues on the MPER helix (25, 38).

Implications for Immunogen Design—Overall our structural data support 2F5 docking to the surface of a kinked MPERp helix exposing the invariable residues Trp-666, Leu-669, Trp-672, and Phe-673, and the putative involvement of the CDR-H3 loop in the process. In previous studies, it was hypothesized that inclusion of residues responsible for the secondary binding process would be required to elicit 2F5-like neutralizing responses (25, 36, 38). To test the immunogenicity of an MPER helix containing all elements involved in epitope recognition by the bNAb2F5, we carried out immunization studies using MPERp as a vaccine. To establish a potential structure-immunogenicity relationship, we monitored conformational changes in the vaccine formulations. IR allows performing reliable measurements (*i.e.* resolution or sensitivity are unaffected) in turbid suspensions such as aggregated membranes and particulate emulsions. Therefore, IR was the technique of choice for confirming the preservation of MPERp helical structures in the viscous media provided by the aluminum salts, "Freund's" water-in-oil emulsion, and membrane adjuvants (Figs. 4*B* and 6).

Even though MPERp dispersed in alum and Freund's adjuvant triggered effective MPER-targeting immunoresponses, the antibodies isolated from these sera were not functional in the cell entry inhibition assays (Fig. 7). It has been reported that interactions of protein antigens with the highly charged aluminum salts may destabilize their structures (81). Consistent with this finding, MPERp in contact with alum underwent significant aggregation, as denoted by the IR absorption at 1620 cm^{-1} (Fig. 4*B, left*). We speculate that MPERp unfolding/aggregation in the highly polar alum medium might result in the presentation of neutralization-irrelevant 2F5 epitope structures to the B-cell receptor. In contrast, IR demonstrated the absence of significant MPERp aggregation in Freund's reverse micelles (Fig. 4*B, right,* and Table 3).

It has been argued that the water molecules confined at the interfacial region of the water-in-oil reverse micelles are non-bulk-like, resulting in a low dielectric environment at the water-oil interface, reminiscent of that found at the membrane-water interface (82). Thus, amphipathic peptides in contact with reverse micelles may attain helical structures compatible with those adopted when adsorbed to membrane surfaces. In particular, this has been demonstrated using IR for the antimicrobial peptide mastoparan X (71). Our results suggest that this is also the case for MPERp in Freund's adjuvant and POPC/Chol/PA vesicles (Table 3). We infer that hydrophobic contacts estab-

lished by MPERp with the oil-water interface may result in limited exposure of the 2F5 epitope key residues to B-cell receptors, in a way comparable with that in contact with the surface of POPC/Chol/PA vesicles (see below).

Given its proximity to the envelope surface and the unusual concentration of aromatic residues, it has been proposed that structuring coupled to membrane partitioning may play a crucial role in determining the structure and orientation of MPER epitopes, which in turn will have an impact on immunogenicity (19, 62, 72, 83). Thus, we studied in parallel the MPERp structure and immunogenicity in two different liposomal formulations (Figs. 5 and 6). 2F5 binding to the POPG-based vaccine was CDR-H3 dependent, whereas the loop was not required for binding to the POPC/Chol/PA-based vaccine (Fig. 5). Thus, only binding to the former correlated with the antibody-neutralizing function. Sustaining different modes of antibody recognition, membrane-bound MPERp helical structures also differed substantially in these vaccines (Fig. 6). The features of the MPERp IR spectrum in POPC/Chol/PA liposomes (Fig. 6*A* and Table 3) resembled the flexibility and solvation degree characteristic of amphipathic helices in contact with membrane surfaces (84). Accordingly, the simulations in the POPC/Chol/PA system disclosed a membrane-bound interfacial helix (Fig. 6*A*). In this structure, 2F5 key epitope residues were engaged in dynamic interactions with membranes and remained mostly inaccessible for binding from solution. Similarly to Freund's, the 2F5-targeting antibodies isolated from the POPC/Chol/PA sera were not functional in cell entry assays (Fig. 7).

We surmise that the conformational flexibility of the interfacial MPERp monomers put forward by the IR and MDS studies, may sustain binding to the membrane-bound MPER epitope by MAb2F5, even in the absence of the CDR-H3 loop (Fig. 5*E*). Thus, the lack of functional antibodies in sera of rabbits immunized with MPERp in Freund's adjuvant and POPC/Chol/PA liposomes (Fig. 7) would be consistent with the activation of B-cell receptors that recognize alternative faces/residues within monomeric, interfacial MPER helices.

Contrasting these observations, the structure adopted by MPERp in the POPG liposomes was devoid of the more flexible conformers and denoted the existence of tightly packed, buried, and solvated helices (Fig. 6*B* and Table 3). MDS further revealed the possibility that a protruding bundle could insert into the lipid bilayer through the C terminus of a peptide monomer and expose to solvent 2F5 key residues from adhered helices (Fig. 6*B*). When used as immunogens, these POPG-bound MPERp structures gave rise to antibodies with a significant capacity of blocking cell infection (Figs. 7 and 8).

We speculate that the efficacy shown by the POPG-MPERp formulation as compared with the other tested vaccines may result from a different pattern of epitope exposure to solvent. Based on the electrostatic repulsion between N-terminal MPERp Glu carboxylates and the acidic phospholipid headgroups, we already anticipated exposure of 2F5 epitope to solvent in this formulation (61). In agreement with our expectations, the N terminus of MPERp never contacted the membrane interface in the MDS (Fig. 6*B*). The liposomal formulation may hypothetically contribute to immunogenicity in other ways. Following recent proposals (25), it is possible that helical bundles protruding from the membrane surface are required to recapitulate antibodies with the capacity for binding 2F5 epitope residues, even if buried within helix-helix contacts. The fact that the 2F5 CDR-H3 was required for binding to POPG-inserted MPERp argues in favor of this possibility (Fig. 5). Alternatively, as also happens in the case detected by MDS, membrane insertion through one monomer might stabilize the out-of-register MPERp helix assembly making possible full exposure of 2F5 epitope residues to solvent in the outermost monomer. The "flagpole"-like MPER structures repeated on the surface of negatively charged membranes, might additionally embody multivalent antigens for the efficient activation of B-cell receptors. Finally, these vesicles might provide a suitable environment for generating antibodies capable of binding heterotypically to peptide and lipid (9, 31).

Although significant (Fig. 8), the inhibitory activity of these antibodies was weak, particularly when compared with that of MAb2F5 (Fig. 5*A*). We note that the former arise from a polyclonal response and that samples containing these antibodies are devoid of the purity level of the isolated mAb. In combination, those two factors are likely to contribute to the reduction of the specific activity of the samples tested here. We also note that to qualify the 2F5-targeting antibodies recovered from the POPG sera as neutralizing antibodies, the neutralization breadth and potency should be evaluated using referenced assays and diverse viral strains and isolates (85). In this regard, an additional study, involving larger numbers of animals and comparing different immunization strategies, is currently under way with the aim to provide evidence for neutralization according to standard methods (86).

In conclusion, results in this work suggest that structural fixation through hydrophobic interactions with the membrane interface may constrain the efficacy of liposomal vaccines targeting the 2F5 epitope. However, they present the possibility that membrane-inserted MPER bundles may embody efficient 2F5-targeting immunogens. Thus, we infer that MPER flagpoles optimized for membrane insertion and/or epitope-exposure functions might exemplify a new paradigm for future design of effective liposomal vaccines targeting the 2F5 epitope.

Acknowledgments—We thank Jean-Philippe Julien and Jamie K. Scott for critical reading of the manuscript. C. D. thankfully acknowledges the computer resources, technical expertise, and assistance provided by the Red Española de Supercomputación and Temple University.

REFERENCES

1. Karlsson Hedestam, G. B., Fouchier, R. A., Phogat, S., Burton, D. R., Sodroski, J., and Wyatt, R. T. (2008) The challenges of eliciting neutralizing antibodies to HIV-1 and to influenza virus. *Nat. Rev. Microbiol.* **6,** 143–155
2. Merk, A., and Subramaniam, S. (2013) HIV-1 envelope glycoprotein structure. *Curr. Opin. Struct. Biol.* **23,** 268–276
3. Melikyan, G. B. (2008) Common principles and intermediates of viral protein-mediated fusion: the HIV-1 paradigm. *Retrovirology* **5,** 111
4. Wyatt, R., and Sodroski, J. (1998) The HIV-1 envelope glycoproteins: fusogens, antigens, and immunogens. *Science* **280,** 1884–1888
5. Blumenthal, R., Durell, S., and Viard, M. (2012) HIV entry and envelope glycoprotein-mediated fusion. *J. Biol. Chem.* **287,** 40841–40849
6. Burton, D. R., Desrosiers, R. C., Doms, R. W., Koff, W. C., Kwong, P. D.,

Moore, J. P., Nabel, G. J., Sodroski, J., Wilson, I. A., and Wyatt, R. T. (2004) HIV vaccine design and the neutralizing antibody problem. *Nat. Immunol.* **5,** 233–236
7. Stamatatos, L., Morris, L., Burton, D. R., and Mascola, J. R. (2009) Neutralizing antibodies generated during natural HIV-1 infection: good news for an HIV-1 vaccine? *Nat. Med.* **15,** 866–870
8. Mascola, J. R., and Montefiori, D. C. (2010) The role of antibodies in HIV vaccines. *Annu. Rev. Immunol.* **28,** 413–444
9. Klein, F., Mouquet, H., Dosenovic, P., Scheid, J. F., Scharf, L., and Nussenzweig, M. C. (2013) Antibodies in HIV-1 vaccine development and therapy. *Science* **341,** 1199–1204
10. Walker, L. M., and Burton, D. R. (2010) Rational antibody-based HIV-1 vaccine design: current approaches and future directions. *Curr. Opin. Immunol.* **22,** 358–366
11. Kwong, P. D., and Mascola, J. R. (2012) Human antibodies that neutralize HIV-1: identification, structures, and B cell ontogenies. *Immunity* **37,** 412–425
12. Gray, E. S., Madiga, M. C., Moore, P. L., Mlisana, K., Abdool Karim, S. S., Binley, J. M., Shaw, G. M., Mascola, J. R., and Morris, L. (2009) Broad neutralization of human immunodeficiency virus type 1 mediated by plasma antibodies against the gp41 membrane proximal external region. *J. Virol.* **83,** 11265–11274
13. Zwick, M. B., Labrijn, A. F., Wang, M., Spenlehauer, C., Saphire, E. O., Binley, J. M., Moore, J. P., Stiegler, G., Katinger, H., Burton, D. R., and Parren, P. W. (2001) Broadly neutralizing antibodies targeted to the membrane-proximal external region of human immunodeficiency virus type 1 glycoprotein gp41. *J. Virol.* **75,** 10892–10905
14. Ofek, G., Tang, M., Sambor, A., Katinger, H., Mascola, J. R., Wyatt, R., and Kwong, P. D. (2004) Structure and mechanistic analysis of the anti-human immunodeficiency virus type 1 antibody 2F5 in complex with its gp41 epitope. *J. Virol.* **78,** 10724–10737
15. Cardoso, R. M., Brunel, F. M., Ferguson, S., Zwick, M., Burton, D. R., Dawson, P. E., and Wilson, I. A. (2007) Structural basis of enhanced binding of extended and helically constrained peptide epitopes of the broadly neutralizing HIV-1 antibody 4E10. *J. Mol. Biol.* **365,** 1533–1544
16. Pejchal, R., Gach, J. S., Brunel, F. M., Cardoso, R. M., Stanfield, R. L., Dawson, P. E., Burton, D. R., Zwick, M. B., and Wilson, I. A. (2009) A conformational switch in human immunodeficiency virus gp41 revealed by the structures of overlapping epitopes recognized by neutralizing antibodies. *J. Virol.* **83,** 8451–8462
17. Zhu, Z., Qin, H. R., Chen, W., Zhao, Q., Shen, X., Schutte, R., Wang, Y., Ofek, G., Streaker, E., Prabakaran, P., Fouda, G. G., Liao, H. X., Owens, J., Louder, M., Yang, Y., Klaric, K. A., Moody, M. A., Mascola, J. R., Scott, J. K., Kwong, P. D., Montefiori, D., Haynes, B. F., Tomaras, G. D., and Dimitrov, D. S. (2011) Cross-reactive HIV-1-neutralizing human monoclonal antibodies identified from a patient with 2F5-like antibodies. *J. Virol.* **85,** 11401–11408
18. Huang, J., Ofek, G., Laub, L., Louder, M. K., Doria-Rose, N. A., Longo, N. S., Imamichi, H., Bailer, R. T., Chakrabarti, B., Sharma, S. K., Alam, S. M., Wang, T., Yang, Y., Zhang, B., Migueles, S. A., Wyatt, R., Haynes, B. F., Kwong, P. D., Mascola, J. R., and Connors, M. (2012) Broad and potent neutralization of HIV-1 by a gp41-specific human antibody. *Nature* **491,** 406–412
19. Montero, M., van Houten, N. E., Wang, X., and Scott, J. K. (2008) The membrane-proximal external region of the human immunodeficiency virus type 1 envelope: dominant site of antibody neutralization and target for vaccine design. *Microbiol. Mol. Biol. Rev.* **72,** 54–84
20. Montero, M., Gulzar, N., Klaric, K. A., Donald, J. E., Lepik, C., Wu, S., Tsai, S., Julien, J. P., Hessell, A. J., Wang, S., Lu, S., Burton, D. R., Pai, E. F., Degrado, W. F., and Scott, J. K. (2012) Neutralizing epitopes in the membrane-proximal external region of HIV-1 gp41 are influenced by the transmembrane domain and the plasma membrane. *J. Virol.* **86,** 2930–2941
21. Muster, T., Steindl, F., Purtscher, M., Trkola, A., Klima, A., Himmler, G., Rüker, F., and Katinger, H. (1993) A conserved neutralizing epitope on gp41 of human immunodeficiency virus type 1. *J. Virol.* **67,** 6642–6647
22. Muster, T., Guinea, R., Trkola, A., Purtscher, M., Klima, A., Steindl, F., Palese, P., and Katinger, H. (1994) Cross-neutralizing activity against divergent human immunodeficiency virus type 1 isolates induced by the gp41 sequence ELDKWAS. *J. Virol.* **68,** 4031–4034
23. Binley, J. M., Wrin, T., Korber, B., Zwick, M. B., Wang, M., Chappey, C., Stiegler, G., Kunert, R., Zolla-Pazner, S., Katinger, H., Petropoulos, C. J., and Burton, D. R. (2004) Comprehensive cross-clade neutralization analysis of a panel of anti-human immunodeficiency virus type 1 monoclonal antibodies. *J. Virol.* **78,** 13232–13252
24. Conley, A. J., Kessler, J. A., 2nd, Boots, L. J., Tung, J. S., Arnold, B. A., Keller, P. M., Shaw, A. R., and Emini, E. A. (1994) Neutralization of divergent human immunodeficiency virus type 1 variants and primary isolates by IAM-41-2F5, an anti-gp41 human monoclonal antibody. *Proc. Natl. Acad. Sci. U.S.A.* **91,** 3348–3352
25. Guenaga, J., and Wyatt, R. T. (2012) Structure-guided alterations of the gp41-directed HIV-1 broadly neutralizing antibody 2F5 reveal new properties regarding its neutralizing function. *PLoS Pathog.* **8,** e1002806
26. Purtscher, M., Trkola, A., Gruber, G., Buchacher, A., Predl, R., Steindl, F., Tauer, C., Berger, R., Barrett, N., and Jungbauer, A. (1994) A broadly neutralizing human monoclonal antibody against gp41 of human immunodeficiency virus type 1. *AIDS Res. Hum. Retroviruses* **10,** 1651–1658
27. Coëffier, E., Clément, J. M., Cussac, V., Khodaei-Boorane, N., Jehanno, M., Rojas, M., Dridi, A., Latour, M., El Habib, R., Barré-Sinoussi, F., Hofnung, M., and Leclerc, C. (2000) Antigenicity and immunogenicity of the HIV-1 gp41 epitope ELDKWA inserted into permissive sites of the MalE protein. *Vaccine* **19,** 684–693
28. McGaughey, G. B., Citron, M., Danzeisen, R. C., Freidinger, R. M., Garsky, V. M., Hurni, W. M., Joyce, J. G., Liang, X., Miller, M., Shiver, J., and Bogusky, M. J. (2003) HIV-1 vaccine development: constrained peptide immunogens show improved binding to the anti-HIV-1 gp41 MAb. *Biochemistry* **42,** 3214–3223
29. Dennison, S. M., Sutherland, L. L., Jaeger, F. H., Anasti, K. M., Parks, R., Stewart, S., Bowman, C., Xia, S. M., Zhang, R., Shen, X., Scearce, R. M., Ofek, G., Yang, Y., Kwong, P. D., Santra, S., Liao, H. X., Tomaras, G., Letvin, N. L., Chen, B., Alam, S. M., and Haynes, B. F. (2011) Induction of antibodies in rhesus macaques that recognize a fusion-intermediate conformation of HIV-1 gp41. *PLoS One* **6,** e27824
30. Guenaga, J., Dosenovic, P., Ofek, G., Baker, D., Schief, W. R., Kwong, P. D., Karlsson Hedestam, G. B., and Wyatt, R. T. (2011) Heterologous epitope-scaffold prime:boosting immuno-focuses B cell responses to the HIV-1 gp41 2F5 neutralization determinant. *PLoS One* **6,** e16074
31. Matyas, G. R., Wieczorek, L., Beck, Z., Ochsenbauer-Jambor, C., Kappes, J. C., Michael, N. L., Polonis, V. R., and Alving, C. R. (2009) Neutralizing antibodies induced by liposomal HIV-1 glycoprotein 41 peptide simultaneously bind to both the 2F5 or 4E10 epitope and lipid epitopes. *AIDS* **23,** 2069–2077
32. Huarte, N., Araujo, A., Arranz, R., Lorizate, M., Quendler, H., Kunert, R., Valpuesta, J. M., and Nieva, J. L. (2012) Recognition of membrane-bound fusion-peptide/MPER complexes by the HIV-1 neutralizing 2F5 antibody: implications for anti-2F5 immunogenicity. *PLoS One* **7,** e52740
33. Joyce, J. G., Hurni, W. M., Bogusky, M. J., Garsky, V. M., Liang, X., Citron, M. P., Danzeisen, R. C., Miller, M. D., Shiver, J. W., and Keller, P. M. (2002) Enhancement of α-helicity in the HIV-1 inhibitory peptide DP178 leads to an increased affinity for human monoclonal antibody 2F5 but does not elicit neutralizing responses *in vitro*. Implications for vaccine design. *J. Biol. Chem.* **277,** 45811–45820
34. Parker, C. E., Deterding, L. J., Hager-Braun, C., Binley, J. M., Schülke, N., Katinger, H., Moore, J. P., and Tomer, K. B. (2001) Fine definition of the epitope on the gp41 glycoprotein of human immunodeficiency virus type 1 for the neutralizing monoclonal antibody 2F5. *J. Virol.* **75,** 10906–10911
35. Barbato, G., Bianchi, E., Ingallinella, P., Hurni, W. H., Miller, M. D., Ciliberto, G., Cortese, R., Bazzo, R., Shiver, J. W., and Pessi, A. (2003) Structural analysis of the epitope of the anti-HIV antibody 2F5 sheds light into its mechanism of neutralization and HIV fusion. *J. Mol. Biol.* **330,** 1101–1115
36. Julien, J. P., Bryson, S., Nieva, J. L., and Pai, E. F. (2008) Structural details of HIV-1 recognition by the broadly neutralizing monoclonal antibody 2F5: epitope conformation, antigen-recognition loop mobility, and anion-binding site. *J. Mol. Biol.* **384,** 377–392
37. Zwick, M. B., Komori, H. K., Stanfield, R. L., Church, S., Wang, M., Parren, P. W., Kunert, R., Katinger, H., Wilson, I. A., and Burton, D. R. (2004) The

long third complementarity-determining region of the heavy chain is important in the activity of the broadly neutralizing anti-human immunodeficiency virus type 1 antibody 2F5. *J. Virol.* **78,** 3155–3161
38. Julien, J. P., Huarte, N., Maeso, R., Taneva, S. G., Cunningham, A., Nieva, J. L., and Pai, E. F. (2010) Ablation of the complementarity-determining region H3 apex of the anti-HIV-1 broadly neutralizing antibody 2F5 abrogates neutralizing capacity without affecting core epitope binding. *J. Virol.* **84,** 4136–4147
39. Sánchez-Martínez, S., Lorizate, M., Katinger, H., Kunert, R., and Nieva, J. L. (2006) Membrane association and epitope recognition by HIV-1 neutralizing anti-gp41 2F5 and 4E10 antibodies. *AIDS Res. Hum. Retroviruses* **22,** 998–1006
40. Kim, M., Sun, Z. Y., Rand, K. D., Shi, X., Song, L., Cheng, Y., Fahmy, A. F., Majumdar, S., Ofek, G., Yang, Y., Kwong, P. D., Wang, J. H., Engen, J. R., Wagner, G., and Reinherz, E. L. (2011) Antibody mechanics on a membrane-bound HIV segment essential for GP41-targeted viral neutralization. *Nat. Struct. Mol. Biol.* **18,** 1235–1243
41. Alam, S. M., Morelli, M., Dennison, S. M., Liao, H. X., Zhang, R., Xia, S. M., Rits-Volloch, S., Sun, L., Harrison, S. C., Haynes, B. F., and Chen, B. (2009) Role of HIV membrane in neutralization by two broadly neutralizing antibodies. *Proc. Natl. Acad. Sci. U.S.A.* **106,** 20234–20239
42. Mirassou, Y., Santiveri, C. M., Pérez de Vega, M. J., González-Muñiz, R., and Jiménez, M. A. (2009) Disulfide bonds *versus* TrpTrp pairs in irregular β-hairpins: NMR structure of vammin loop 3-derived peptides as a case study. *ChemBioChem* **10,** 902–910
43. Cornilescu, G., Delaglio, F., and Bax, A. (1999) Protein backbone angle restraints from searching a database for chemical shift and sequence homology. *J. Biomol. NMR* **13,** 289–302
44. Güntert, P., Mumenthaler, C., and Wüthrich, K. (1997) Torsion angle dynamics for NMR structure calculation with the new program DYANA. *J. Mol. Biol.* **273,** 283–298
45. Güntert, P. (2004) Automated NMR structure calculation with CYANA. *Methods Mol. Biol.* **278,** 353–378
46. Laskowski, R. A., Rullmannn, J. A., MacArthur, M. W., Kaptein, R., and Thornton, J. M. (1996) AQUA and PROCHECK-NMR: programs for checking the quality of protein structures solved by NMR. *J. Biomol. NMR* **8,** 477–486
47. Koradi, R., Billeter, M., and Wüthrich, K. (1996) MOLMOL: a program for display and analysis of macromolecular structures. *J. Mol. Graph.* **14,** 51-**55**
48. Guex, N., and Peitsch, M. C. (1997) SWISS-MODEL and the Swiss-Pdb-Viewer: an environment for comparative protein modeling. *Electrophoresis* **18,** 2714–2723
49. Yethon, J. A., Epand, R. F., Leber, B., Epand, R. M., and Andrews, D. W. (2003) Interaction with a membrane surface triggers a reversible conformational change in Bax normally associated with induction of apoptosis. *J. Biol. Chem.* **278,** 48935–48941
50. Arrondo, J. L., and Goñi, F. M. (1999) Structure and dynamics of membrane proteins as studied by infrared spectroscopy. *Prog. Biophys. Mol. Biol.* **72,** 367–405
51. Phillips, J. C., Braun, R., Wang, W., Gumbart, J., Tajkhorshid, E., Villa, E., Chipot, C., Skeel, R. D., Kalé, L., and Schulten, K. (2005) Scalable molecular dynamics with NAMD. *J. Comput. Chem.* **26,** 1781–1802
52. MacKerell, A. D., Bashford, D., Bellott, Dunbrack, R. L., Evanseck, J. D., Field, M. J., Fischer, S., Gao, J., Guo, H., Ha, S., Joseph-McCarthy, D., Kuchnir, L., Kuczera, K., Lau, F. T. K., Mattos, C., Michnick, S., Ngo, T., Nguyen, D. T., Prodhom, B., Reiher, W. E., Roux, B., Schlenkrich, M., Smith, J. C., Stote, R., Straub, J., Watanabe, M., Wiórkiewicz-Kuczera, J., Yin, D., and Karplus, M. (1998) All-atom empirical potential for molecular modeling and dynamics studies of proteins. *J. Phys. Chem. B* **102,** 3586–3616
53. Klauda, J. B., Venable, R. M., Freites, J. A., O'Connor, J. W., Tobias, D. J., Mondragon-Ramirez, C., Vorobyov, I., MacKerell, A. D., Jr., and Pastor, R. W. (2010) Update of the CHARMM all-atom additive force field for lipids: validation on six lipid types. *J. Phys. Chem. B.* **114,** 7830–7843
54. Jorgensen, W. L., Chandrasekhar, J., Madura, J. D., Impey, R. W., and Klein, M. L. (1983) Comparison of simple potential functions for simulating liquid water. *J. Chem. Phys.* **79,** 926–935
55. Cournia, Z., Smith, J. C., and Ullmann, G. M. (2005) A molecular mechanics force field for biologically important sterols. *J. Comput. Chem.* **26,** 1383–1399
56. Martyna, G. J., Tobias, D. J., and Klein, M. L. (1994) Constant pressure molecular dynamics algorithms. *J. Chem. Phys.* **101,** 4177–4189
57. Feller, S. E., Zhang, Y., Pastor, R. W., and Brooks, B. R. (1995) Constant pressure molecular dynamics simulation:the Langevin piston method. *J. Chem. Phys.* **103,** 4613–4621
58. Essmann, U., Perera, L., and Berkowitz, M. (1995) A smooth particle mesh Ewald method. *J. Chem. Phys.* **103,** 8577–8593
59. Miyamoto, S., and Kollman, P. (1992) Settle: an analytical version of the SHAKE and RATTLE algorithm for rigid water models. *J. Comput. Chem.* **13,** 952–962
60. Dreesman, G. R., Sanchez, Y., Ionescu-Matiu, I., Sparrow, J. T., Six, H. R., Peterson, D. L., Hollinger, F. B., and Melnick, J. L. (1982) Antibody to hepatitis B surface antigen after a single inoculation of uncoupled synthetic HBsAg peptides. *Nature* **295,** 158–160
61. Maeso, R., Huarte, N., Julien, J. P., Kunert, R., Pai, E. F., and Nieva, J. L. (2011) Interaction of anti-HIV type 1 antibody 2F5 with phospholipid bilayers and its relevance for the mechanism of virus neutralization. *AIDS Res. Hum. Retroviruses* **27,** 863–876
62. Alving, C. R., Rao, M., Steers, N. J., Matyas, G. R., and Mayorov, A. V. (2012) Liposomes containing lipid A: an effective, safe, generic adjuvant system for synthetic vaccines. *Expert Rev. Vaccines* **11,** 733–744
63. Menendez, A., Chow, K. C., Pan, O. C., and Scott, J. K. (2004) Human immunodeficiency virus type 1-neutralizing monoclonal antibody 2F5 is multispecific for sequences flanking the DKW core epitope. *J. Mol. Biol.* **338,** 311–327
64. Wuthrich, K. (1986) *NMR of Proteins and Nucleic Acids.* John Wiley & Sons, Inc., New York
65. Wüthrich, K., Billeter, M., and Braun, W. (1984) Polypeptide secondary structure determination by nuclear magnetic resonance observation of short proton-proton distances. *J. Mol. Biol.* **180,** 715–740
66. Wishart, D. S., Bigam, C. G., Holm, A., Hodges, R. S., and Sykes, B. D. (1995) ^{1}H, ^{13}C, and ^{15}N random coil NMR chemical shifts of the common amino acids. I. Investigations of nearest-neighbor effects. *J. Biomol. NMR* **5,** 67–81
67. Reisdorf, W. C., Jr., and Krimm, S. (1996) Infrared amide I′ band of the coiled coil. *Biochemistry* **35,** 1383–1386
68. Walsh, S. T., Cheng, R. P., Wright, W. W., Alonso, D. O., Daggett, V., Vanderkooi, J. M., and DeGrado, W. F. (2003) The hydration of amides in helices; a comprehensive picture from molecular dynamics, IR, and NMR. *Protein Sci.* **12,** 520–531
69. Vu, D. M., Myers, J. K., Oas, T. G., and Dyer, R. B. (2004) Probing the folding and unfolding dynamics of secondary and tertiary structures in a three-helix bundle protein. *Biochemistry* **43,** 3582–3589
70. Coffman, R. L., Sher, A., and Seder, R. A. (2010) Vaccine adjuvants: putting innate immunity to work. *Immunity* **33,** 492–503
71. Mukherjee, S., Chowdhury, P., DeGrado, W. F., and Gai, F. (2007) Site-specific hydration status of an amphipathic peptide in AOT reverse micelles. *Langmuir* **23,** 11174–11179
72. Lorizate, M., Huarte, N., Sáez-Cirión, A., and Nieva, J. L. (2008) Interfacial pre-transmembrane domains in viral proteins promoting membrane fusion and fission. *Biochim. Biophys. Acta* **1778,** 1624–1639
73. Sun, Z. Y., Oh, K. J., Kim, M., Yu, J., Brusic, V., Song, L., Qiao, Z., Wang, J. H., Wagner, G., and Reinherz, E. L. (2008) HIV-1 broadly neutralizing antibody extracts its epitope from a kinked gp41 ectodomain region on the viral membrane. *Immunity* **28,** 52–63
74. Suárez, T., Gallaher, W. R., Agirre, A., Goñi, F. M., and Nieva, J. L. (2000) Membrane interface-interacting sequences within the ectodomain of the human immunodeficiency virus type 1 envelope glycoprotein: putative role during viral fusion. *J. Virol.* **74,** 8038–8047
75. Biron, Z., Khare, S., Samson, A. O., Hayek, Y., Naider, F., and Anglister, J. (2002) A monomeric 3_{10}-helix is formed in water by a 13-residue peptide representing the neutralizing determinant of HIV-1 on gp41. *Biochemistry* **41,** 12687–12696
76. Schibli, D. J., Montelaro, R. C., and Vogel, H. J. (2001) The membrane-proximal tryptophan-rich region of the HIV glycoprotein, gp41, forms a

well defined helix in dodecylphosphocholine micelles. *Biochemistry* **40,** 9570–9578
77. Coutant, J., Yu, H., Clément, M. J., Alfsen, A., Toma, F., Curmi, P. A., and Bomsel, M. (2008) Both lipid environment and pH are critical for determining physiological solution structure of 3-D-conserved epitopes of the HIV-1 gp41-MPER peptide P1. *FASEB J.* **22,** 4338–4351
78. Bryson, S., Julien, J. P., Hynes, R. C., and Pai, E. F. (2009) Crystallographic definition of the epitope promiscuity of the broadly neutralizing anti-human immunodeficiency virus type 1 antibody 2F5: vaccine design implications. *J. Virol.* **83,** 11862–11875
79. Depetris, R. S., Julien, J. P., Khayat, R., Lee, J. H., Pejchal, R., Katpally, U., Cocco, N., Kachare, M., Massi, E., David, K. B., Cupo, A., Marozsan, A. J., Olson, W. C., Ward, A. B., Wilson, I. A., Sanders, R. W., and Moore, J. P. (2012) Partial enzymatic deglycosylation preserves the structure of cleaved recombinant HIV-1 envelope glycoprotein trimers. *J. Biol. Chem.* **287,** 24239–24254
80. Julien, J. P., Cupo, A., Sok, D., Stanfield, R. L., Lyumkis, D., Deller, M. C., Klasse, P. J., Burton, D. R., Sanders, R. W., Moore, J. P., Ward, A. B., and Wilson, I. A. (2013) Crystal structure of a soluble cleaved HIV-1 envelope trimer. *Science* **342,** 1477–1483
81. Jones, L. S., Peek, L. J., Power, J., Markham, A., Yazzie, B., and Middaugh, C. R. (2005) Effects of adsorption to aluminum salt adjuvants on the structure and stability of model protein antigens. *J. Biol. Chem.* **280,** 13406–13414
82. Dokter, A. M., Woutersen, S., and Bakker, H. J. (2006) Inhomogeneous dynamics in confined water nanodroplets. *Proc. Natl. Acad. Sci. U.S.A.* **103,** 15355–15358
83. Zwick, M. B. (2005) The membrane-proximal external region of HIV-1 gp41: a vaccine target worth exploring. *Aids* **19,** 1725–1737
84. Haris, P. I., Ramesh, B., Brazier, S., and Chapman, D. (1994) The conformational analysis of a synthetic S4 peptide corresponding to a voltage-gated potassium ion channel protein. *FEBS Lett.* **349,** 371–374
85. Polonis, V. R., Brown, B. K., Rosa Borges, A., Zolla-Pazner, S., Dimitrov, D. S., Zhang, M. Y., Barnett, S. W., Ruprecht, R. M., Scarlatti, G., Fenyö, E. M., Montefiori, D. C., McCutchan, F. E., and Michael, N. L. (2008) Recent advances in the characterization of HIV-1 neutralization assays for standardized evaluation of the antibody response to infection and vaccination. *Virology* **375,** 315–320
86. Gulzar, N., Klaric, K., Parfyonov, M., Montero, M., Wang, S., Huarte, N., Appellaniz, B., Nieva, J., Lu, S., and Scott, J. (2013) Study 1: Optimizing vaccines that target the 2F5 epitope of the membrane proximal external region of HIV-1 gp41. *AIDS Res. Hum. Retroviruses* **29,** 13–63

Supplemental Data:

Structure and Immunogenicity of a Peptide Vaccine Including the Complete HIV-1 gp41 2F5 Epitope. Implications for Antibody Recognition Mechanism and Immunogen Design

Soraya Serrano, Aitziber Araujo, Beatriz Apellániz, Steve Bryson, Pablo Carravilla, Igor de la Arada, Nerea Huarte, Edurne Rujas, Emil F. Pai, José L.R. Arrondo, Carmen Domene, María Angeles Jiménez, and José L. Nieva

Table S1. ^{1}H chemical shifts (ppm, from DSS) for peptide MPERp in a H_2O/D_2O (9:1 ratio by volume) solution containing 20 mM deuterated dodecylphosphocholine (DPC) and 2 mM HEPES buffer at pH 7.0 and 25ºC. Those ^{13}C chemical shifts that could be unambiguously assigned from a 2D $^{1}H,^{13}C$-HSQC recorded at natural ^{13}C abundance are listed in italics. Those methylene protons (β or γ) and Leu methyl groups that were stereo-specifically assigned are indicated by an asterisk.

Residue	HN	$C_\alpha H$	$C_\beta H$	Others
Asn 1		4.14	2.89, 2.89	$N_\delta H_2$ 6.99, 7.70
Glu 2		4.26	1.98, 2.08	$C_{\gamma\gamma'}H$ 2.29, 2.29, *33.9*
Gln 3	8.41	4.25	2.03, 2.09	$C_{\gamma\gamma'}H$ 2.36, 2.36; $N_\varepsilon H_2$ 6.85, 7.63
Glu 4	8.32	4.25	1.96, 2.04	$C_{\gamma\gamma'}H$ 2.26, 2.26, *36.4*
Leu 5	8.29	4.27	1.58, 1.71	$C_\gamma H$ 1.67; $C_\delta H_3$ 0.87, *23.8*; $C_{\delta'}H_3$ 0.92, *25.1*
Leu 6	8.06	4.36	1.56, 1.66	$C_\gamma H$ 1.61; $C_\delta H_3$ 0.83, *23.8*; $C_{\delta'}H_3$ 0.87, *25.2*
Glu 7	8.25	4.32	1.98, 2.09*	$C_{\gamma\gamma'}H$ 2.23, 2.29, *36.4*
Leu 8	8.29	4.18	1.61, 1.71*	$C_\gamma H$ 1.71; $C_\delta H_3$ 0.84, *23.8*; $C_{\delta'}H_3$ 0.92, *25.1*
Asp 9	8.48	4.50	2.72, 2.72	
Lys 10	8.08	4.08	1.72, 1.63*	$C_{\gamma\gamma'}H$ 1.16, 1.16; $C_{\delta\delta'}H$ 1.51, 1.51; $C_{\varepsilon\varepsilon'}H$ 2.80, 2.80, *41.6*
Trp 11	7.94	4.53	3.43, 3.24*	$C_{\delta1}H$ 7.38; $N_{\varepsilon1}H$ 10.65; $C_{\varepsilon3}H$ 7.51; $C_{\zeta3}H$ 6.92; $C_{\eta2}H$ 7.06; $C_{\zeta2}H$ 7.42
Ala 12	8.11	4.08	1.51, *18.5*	
Ser 13	8.10	4.31	3.90, 3.98	
Leu 14	7.83	4.15	1.79, 1.65*	$C_\gamma H$ 1.66; $C_\delta H_3$ 0.79*; $C_{\delta'}H_3$ 0.85*
Trp 15	7.94	4.59	3.43, 3.24*	$C_{\delta1}H$ 7.25; $N_{\varepsilon1}H$ 10.30; $C_{\varepsilon3}H$ 7.54; $C_{\zeta3}H$ 6.91; $C_{\eta2}H$ 7.04; $C_{\zeta2}H$ 7.41
Asn 16	8.02	4.58	2.82, 2.88	$N_\delta H_2$ 7.00, 7.63
Trp 17	nd	4.37	3.31, 3.31	$C_{\delta1}H$ 7.18; $N_{\varepsilon1}H$ 10.50; $C_{\varepsilon3}H$ 7.36; $C_{\zeta3}H$ 6.91; $C_{\eta2}H$ 7.06; $C_{\zeta2}H$ 7.44
Phe 18	7.98	4.22	2.95, 3.10*	$C_{\delta\delta'}H$ 7.21, 7.21; $C_{\varepsilon\varepsilon'}H$ 7.12, 7.12; $C_\zeta H$ nd
Asn 19	7.64	4.55	2.62, 2.81	$N_\delta H_2$ 7.67, 6.70*

Ile 20	8.12	3.67	1.61	$C_{\gamma\gamma'}H$ 1.14, 1.42*; $C_{\gamma}H_3$ 0.76, *17.8*; $C_{\delta}H_3$ 0.75, *13.5*
Thr 21	8.03	3.85	4.02	$C_{\gamma}H_3$ 1.05, *21.9*
Asn 22	7.90	4.57	2.69, 2.69	$N_{\delta}H_2$ 6.70, 7.59
Trp 23	7.99	4.58	3.33, 3.33	$C_{\delta 1}H$ 7.19; $N_{\varepsilon 1}H$ 10.27; $C_{\varepsilon 3}H$ 7.42; $C_{\zeta 3}H$ 6.85; $C_{\eta 2}H$ 6.98; $C_{\zeta 2}H$ 7.33
Leu 24	8.23	4.03	1.50, 1.79*	$C_{\gamma}H$ 1.79; $C_{\delta}H_3$ 0.91*; $C_{\delta'}H_3$ 0.85*
Trp 25	7.93	4.26	3.33, 3.33	$C_{\delta 1}H$ 7.16; $N_{\varepsilon 1}H$ 10.24; $C_{\varepsilon 3}H$ 7.45; $C_{\zeta 3}H$ 7.06; $C_{\eta 2}H$ 7.21; $C_{\zeta 2}H$ 7.49
Tyr 26	7.74	4.00	3.00, 3.12	$C_{\delta\delta'}H$ 7.09, 7.09; $C_{\varepsilon\varepsilon'}H$ 6.81, 6.81
Ile 27	7.83	3.77	1.92	$C_{\gamma\gamma'}H$ 1.64, 1.30*; $C_{\gamma}H_3$ 0.90, *18.2*; $C_{\delta}H_3$ 0.88, *13.7*
Lys 28	7.69	4.04	1.73, 1.80	$C_{\gamma\gamma'}H$ 1.41, 1.47; $C_{\delta\delta'}H$ 1.58, 1.58; $C_{\varepsilon\varepsilon'}H$ 2.81, 2.81, *41.6*
$CONH_2$	*6.96, 7.26*			

Table S2. ^{1}H chemical shifts (ppm, from DSS) for peptide MPERp in a H_2O/D_2O (9:1 ratio by volume) solution containing 2 mM HEPES buffer at pH 7.0, and 25 % HFIP at 25ºC. Those ^{13}C chemical shifts that could be unambiguously assigned from a 2D $^{1}H,^{13}C$-HSQC recorded at natural ^{13}C abundance are listed in italics. An asterisk indicates the stereo-specifically assigned methylene protons. nd stands for not determined.

Residue	HN	$C_\alpha H$	$C_\beta H$	Others
Asn 1		nd	3.21, 3.36, *37.0*	$N_\delta H_2$ 6.99, 7.72
Glu 2		4.17	2.15, 2.15	$C_{\gamma\gamma'}H$ 2.49, 2.49, *33.9*
Gln 3	8.34	4.04	2.15, 2.18	$C_{\gamma\gamma'}H$ 2.46, 2.46, *33.9*; $N_\varepsilon H_2$ nd
Glu 4	8.09	4.09	2.13, 2.20	$C_{\gamma\gamma'}H$ 2.45, 2.52, *33.7*
Leu 5	7.56	4.22	1.77, 1.83	$C_\gamma H$ 1.76; $C_\delta H_3$ 0.93, *23.1*; $C_{\delta'}H_3$ 0.99, *23.7*
Leu 6	7.91	4.18	1.65, 1.93	$C_\gamma H$ 1.83; $C_\delta H_3$ 0.84, *23.5*; $C_{\delta'}H_3$ 0.97, *24.3*
Glu 7	7.92	4.17	2.21, 2.27	$C_{\gamma\gamma'}H$ 2.49, 2.58, *34.4*
Leu 8	8.17	4.30	1.88, 1.88	$C_\gamma H$ 1.83; $C_\delta H_3$ 0.94, *22.5*; $C_{\delta'}H_3$ 1.00, *23.5*
Asp 9	8.48	4.50	2.92, 3.01	
Lys 10	8.17	4.09	2.00, 2.07	$C_{\gamma\gamma'}H$ 1.42, 1.60; $C_{\delta\delta'}H$ 1.68, 1.68; $C_{\varepsilon\varepsilon'}H$ 2.88, 2.88, *42.1*
Trp 11	8.33	4.48	3.40, 3.51	$C_{\delta1}H$ 7.11; $N_{\varepsilon1}H$ 9.06; $C_{\varepsilon3}H$ 7.64; $C_{\zeta3}H$ 7.04; $C_{\eta2}H$ 6.97; $C_{\zeta2}H$ 7.11
Ala 12	9.12	3.98	1.61, *17.6*	
Ser 13	8.15	4.32	nd	
Leu 14	7.99	4.29	1.73, 1.83	$C_\gamma H$ 1.71; $C_\delta H_3$ *0.88*, *23.4*; $C_{\delta'}H_3$ 0.92, *23.8*
Trp 15	8.61	4.39	2.80, 3.13	$C_{\delta1}H$ 7.25; $N_{\varepsilon1}H$ 8.96; $C_{\varepsilon3}H$ 7.52; $C_{\zeta3}H$ 7.06; $C_{\eta2}H$ 7.24; $C_{\zeta2}H$ 7.44
Asn 16	8.46	4.42	2.77, 3.08	$N_\delta H_2$ 6.34, 7.37
Trp 17	8.30	4.36	3.42, 3.59*	$C_{\delta1}H$ 7.01; $N_{\varepsilon1}H$ 9.02; $C_{\varepsilon3}H$ 7.57; $C_{\zeta3}H$ 7.06; $C_{\eta2}H$ 7.18; $C_{\zeta2}H$ 7.36
Phe 18	9.14	3.84	3.12, 3.21	$C_{\delta\delta'}H$ 7.09, 7.09; $C_{\varepsilon\varepsilon'}H$ 7.29, 7.29; $C_\zeta H$ nd
Asn 19	7.98	4.20	2.39, 2.66	$N_\delta H_2$ nd

Ile 20	8.45	3.83	1.82	$C_{\gamma\gamma'}H$ 1.14, 1.70; $C_{\gamma}H_3$ 0.93, *16.6*; $C_{\delta}H_3$ 0.85, *12.4*
Thr 21	7.98	3.73	3.71	$C_{\gamma}H_3$ 0.70, *20.4*
Asn 22	7.62	4.44	2.47, 2.65	$N_{\delta}H_2$ 5.32, 6.73
Trp 23	7.99		3.34, 3.53	$C_{\delta 1}H$ 7.09; $N_{\varepsilon 1}H$ 9.09; $C_{\varepsilon 3}H$ 7.57; $C_{\zeta 3}H$ 7.01; $C_{\eta 2}H$ 7.17; $C_{\zeta 2}H$ 7.36
Leu 24	8.46	3.87	1.84, 1.40*	$C_{\gamma}H$ 1.85; $C_{\delta}H_3$ 0.84, *22.4*; $C_{\delta'}H_3$ 0.86, *24.4*
Trp 25	8.11	4.20	3.27, 3.32	$C_{\delta 1}H$ 6.96; $N_{\varepsilon 1}H$ 9.41; $C_{\varepsilon 3}H$ 7.49; $C_{\zeta 3}H$ 7.11; $C_{\eta 2}H$ 7.22; $C_{\zeta 2}H$ 7.42
Tyr 26	7.83	4.09	3.00, 3.11	$C_{\delta\delta'}H$ 7.06, 7.06; $C_{\varepsilon\varepsilon'}H$ 6.85, 6.85
Ile 27	8.11	3.73	1.70	$C_{\gamma\gamma'}H$ 1.10, 1.23; $C_{\gamma}H_3$ 0.66, *17.0*; $C_{\delta}H_3$ 0.65, *11.8*
Lys 28	8.00	4.03	1.78, 1.78	$C_{\gamma\gamma'}H$ 1.39, 1.39; $C_{\delta\delta'}H$ 1.58, 1.58; $C_{\varepsilon\varepsilon'}H$ 2.84, 2.84, *41.8*
$CONH_2$	*6.66, 6.92*			

Structure and Immunogenicity of a Peptide Vaccine, Including the Complete HIV-1 gp41 2F5 Epitope: IMPLICATIONS FOR ANTIBODY RECOGNITION MECHANISM AND IMMUNOGEN DESIGN

Soraya Serrano, Aitziber Araujo, Beatriz Apellániz, Steve Bryson, Pablo Carravilla, Igor de la Arada, Nerea Huarte, Edurne Rujas, Emil F. Pai, José L. R. Arrondo, Carmen Domene, María Angeles Jiménez and José L. Nieva

J. Biol. Chem. 2014, 289:6565-6580.
doi: 10.1074/jbc.M113.527747 originally published online January 15, 2014
